Fall 2007

Study of interaction between indium species and DNA in the formation of DNA -templated nanowires

Shivashankar Suryanarayanan
Louisiana Tech University

STUDY OF INTERACTION BETWEEN INDIUM SPECIES AND

DNA IN THE FORMATION OF DNA-TEMPLATED

NANOWIRES

By

Shivashankar Suryanarayanan, BE

A Dissertation Presented in Partial Fulfillment of
the Requirement for the Degree
Doctor of Philosophy

COLLEGE OF ENGINEERING AND SCIENCE
LOUISIANA TECH UNIVERSITY

November 2007

UMI Number: 3285243

INFORMATION TO USERS

The quality of this reproduction is dependent upon the quality of the copy submitted. Broken or indistinct print, colored or poor quality illustrations and photographs, print bleed-through, substandard margins, and improper alignment can adversely affect reproduction.

In the unlikely event that the author did not send a complete manuscript and there are missing pages, these will be noted. Also, if unauthorized copyright material had to be removed, a note will indicate the deletion.

UMI®

LOUISIANA TECH UNIVERSITY

THE GRADUATE SCHOOL

10/26/07
_____
Date

We   hereby   recommend   that   the   dissertation   prepared   under   our   supervision

by Shivashankar Suryanarayanan

entitled Study of Interaction Between Indium Species and DNA

in the Formation of DNA-Templated Nanowires

_____

_____

be   accepted   in   partial   fulfillment   of   the   requirements   for   the   Degree   of

Ph.D. in Engineering

_____
Supervisor of Dissertation Research

_____
Head of Department

_____
Department

Recommendation concurred in:

_____

_____

_____

Advisory Committee

_____

Approved:

_____
Director of Graduate Studies

Approved:

_____
Dean of the Graduate School

_____
Dean of the College

GS Form 13a
(6/07)

ABSTRACT

A primary goal of semiconductor industry is to improve device performance and capability by downscaling feature size and upscaling packaging density. As optical-lithography, the mainstream technology for microfabrication, is being stretched to its limit, new unconventional fabrication techniques are being explored as alternatives. A "Bottom-up" approach for manufacturing is emerging as an answer to limitations posed by the traditional "Top-down" approach. Nanowires, bearing the potential of being the basic building blocks for such an approach, are gaining tremendous attention in nanoelectronics. Metal nanowires fabricated using DNA as templates have potential for precise control of length, diameter and positioning. However, wires formed by assembly of metal nanostructures were found to have considerably high electrical resistivity. Oxide formation, irregular structure and formation of grain boundaries in metal nanostructure can be attributed to this problem.

This dissertation is an investigation into factors that affect the formation of DNA templated indium nanowires. They could be treated thermally to increase overall electrical conductivity by utilizing the low melting point of the metal. We have used indium(0), (I) and (III) species as precursors to DNA metallization. Indium(0) in the form of nanoparticles was prepared by reducing indium(I) complex to indium(0). A organic complex {[HB(3-phpz)$_3$]In} was synthesized to stabilize otherwise highly air-sensitive

iii

indium(I) species derived from cyclopentadine. Indium(III) species in the form of aqueous indium trichloride was also used.

During the interaction studies of indium species with DNA, we found that indium(III) binds to DNA in aqueous medium inducing conformal changes and considerable coiling and condensation of DNA molecules, making it unsuitable for nanowire preparation. Indium nanoparticles did not selectively deposit on DNA, indicating that indium(0) has no specific affinity towards DNA molecules. However, reduction of {[HB(3-phpz)$_3$]In} using sodium in the presence of DNA shows successful metallization of DNA. Even though laterally stretched wires with uniform diameter were not formed, selective deposition of indium metal on DNA, forming random network of metallized DNA bundles with diameters between 20-100 nm was accomplished. Preliminary investigation on electrical resistivity indicates that heat treatment of the nanowires reduces the resistivity of these wires by a factor of five.

In the future, it will be possible to assemble nanowires with better orientation, higher uniformity and lower diameters by applying the knowledge gained during this study to already existing techniques of DNA templated nanowire assembly. Indium nanowires thus assembled can be feasibly heat-treated to achieve highly uniform structure with low resistively making it compatible as a component for futuristic nanocircuits.

APPROVAL FOR SCHOLARLY DISSEMINATION

The author grants to the Prescott Memorial Library of Louisiana Tech University the right to reproduce, by appropriate methods, upon request, any or all portions of this Dissertation. It is understood that "proper request" consists of the agreement, on the part of the requesting party, that said reproduction is for his personal use and that subsequent reproduction will not occur without written approval of the author of this Dissertation. Further, any portions of the Dissertation used in books, papers, and other works must be appropriately referenced to this Dissertation.

Finally, the author of this Dissertation reserves the right to publish freely, in the literature, at any time, any or all portions of this Dissertation.

Author

Date   11/01/2007

TABLE OF CONTENTS

LIST OF TABLES

LIST OF FIGURES

ix

ACKNOWLEDGMENTS

I sincerely thank Dr. Donald T. Haynie and Dr. Upali Siriwardane for their invaluable guidance, encouragement, and generous support throughout the project. Without their help I could not have finished this project. I am grateful to Dr. Hisham Hegab, Dr. Rastko Selmic and Dr. Tabbetha Dobbins for being on my advisory committee. I also thank my group members Dr. Qun Gu, Dr. Chuanding Cheng and Ravikant Gonela for their valuable guidance and discussions. I thank Dr. Alfred Gunasekaran and Dr. Xiaohe Xu for their help with SEM characterizations. I also thank Dr. L. D. Snow, Mr. Danny Eddy and Dr. Marilyn Cox for their guidance in chemistry.

I would also like to thank Shrijit, Sachin, Kriti, Ninad, Kunal, Vikram, Vishnu, Vikrant, and other friends for their constant support and encouragement. I am deeply indebted to my parents for their constant encouragement and blessings which always gave me strength to pursue a successful career and completion of the degree. Finally, I wish to dedicate this dissertation and all my research work to my family, for they have never lost faith in me.

CHAPTER 1

INTRODUCTION

In the modern world, the quest for development of better materials, techniques, and ultimately, products, has been driven by the need for continued betterment of humankind. From the invention of vacuum diodes, all the way up to the present fastest supercomputer (IBM®, capable of performing up to 12.3 trillion operations per second), the key for progress has been a scientific problem-solving approach coupled with innovation. Systems developed as a result of such a process supersede the previous systems and render them obsolete. However, all systems do have certain shortcomings which open a large window for improvement. This deficiency eventually leads to to the need for development of a more advanced system. Scientific research aims at identifying these shortcomings and addressing the problems in a creative and systematic fashion, based upon knowledge acquired and documented over time. In the semiconductor industry, fabrication in micro-scale has been traditionally carried out using the "top-down" approach. This approach basically involves building something by starting with a larger component and carving away material until the desired shape and size is achieved. This method can be compared with sculpting from a block of stone. This approach has evolved significantly over the last few decades enabling continuous miniaturization of the devices. However it has its own limitations which will be discussed latter in this chapter. In his classic talk titled "There's plenty of room at the bottom" (December 29, 1959 at

1

annual meeting of American Physical Society) Richard P. Feynman, the Nobel laureate of physics described a field in which little had been done, but in which an enormous amount could be done in principle. He proposed a "bottom-up" approach of manufacturing which involves manipulation of basic building blocks of matter (atoms and molecules) to achieve desired shape and size. In this dissertation, a similar approach towards fabricating metal nanowires using DNA molecules as template and metal ions as the basic building blocks has been applied. These wires can play a crucial role as interconnects in futuristic nanocircuits.

1.1 Micro-Fabrication

Micro-fabrication is a collective term for the technologies applied in fabrication of components in the micrometer regime. The applications of micro-fabrication can be classified into microelectronics, micromechanics, micro-optics, microfluidics and micropackaging. Two or more of these microsystems often come together to form advanced functional systems. Fabricating microsystems from silicon wafers is being used for developing devices such as transistors, Integrated Circuits (ICs) and Micro Electro Mechanical Systems (MEMS). These devices constitute the basic components of almost all electronic devices (such as radio, television, computers, etc.) available currently.

A pattern from a master (known as a mask) is transferred onto the silicon wafer by a process called photolithography (or optical lithography), enabling mass production of components. Optical lithography has been the mainstream technology in semiconductor industry since late 1950s, when ICs were first invented. The mask contains the details of the devices being fabricated and the layout of the circuit. Typically, patterns from more than one mask are superimposed on the wafer to achieve

the desired configuration. The basic steps involved in the photolithography process are as follows: 1) mask printing; 2) coating photoresist on the wafer; 3) exposing; 4) developing; and 5) etching. A schematic of exposure, developing and etching steps involved in simple pattern transfer from a mask onto a silicon wafer is shown in Figure 1.1. Basic factors controlling the minimum feature size of the pattern are mask design, pattern transfer method, photoresist properties and the wavelength of light. The mask is printed using a pattern generator. Commonly-used pattern generators include: 1) plotters; 2) optical pattern generators; and 3) electron beam pattern generators. Contact printing, proximity printing and projection printing are the three basic types of pattern transfer techniques traditionally used. Photoresists are usually photosensitive polymers which become either more soluble (positive) or less soluble (negative) in a developer solution upon exposure to specific wavelengths of light. The chemical properties of the photoresist determine how accurately the transition occurs upon exposure. Finally, the wavelength of the exposure light is critical in photolithography process. The smaller the wavelength of the light is, the smaller is the feature size that can be achieved.
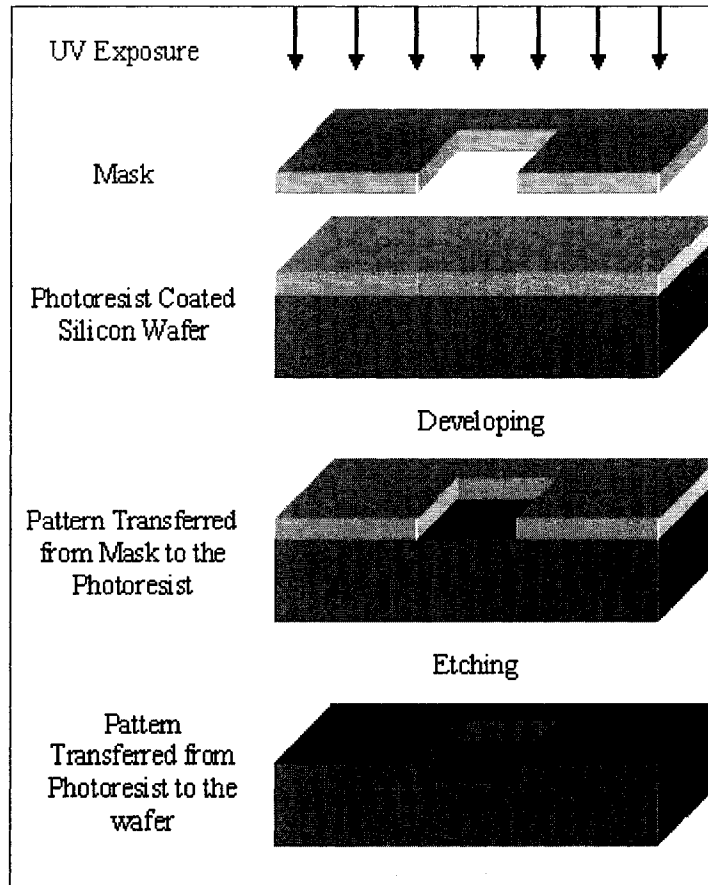
Figure 1.1 Schematic of steps in photolithography (Exposure, developing and etching).

Electron Beam Lithography (EBL) is a technique similar to photolithography. EBL uses a focused beam of electrons to form the circuit patterns on the photoresist, as opposed to using light for the same purpose in optical lithography. Electron lithography uses shorter wavelength (employing 10-50 keV electrons) offering higher patterning resolution than optical lithography. EBL traces the pattern directly on to the resist-coated wafer using an electron beam as its drawing pen eliminating the requirement of masks. However, the high power requirement of the electron beams makes it difficult to control. Moreover, this method is slow as compared with photolithography, making it undesirable when mass production is required.

1.2 Lithography Challenges

In 1965, Intel® co-founder Dr. Gordon Moore predicted the trend for development of semiconductor industry. His prediction, now popularly known as Moore's Law, states that the number of transistors on a chip doubles about every two years. Keeping up with this law has been the main goal of semiconductor industry since then. Continuous improvement of lithography over the past three decades has been able to keep up with the predicted trend so far. Figure 1.2 shows the comparison between Moore's law prediction and actual observed trend.
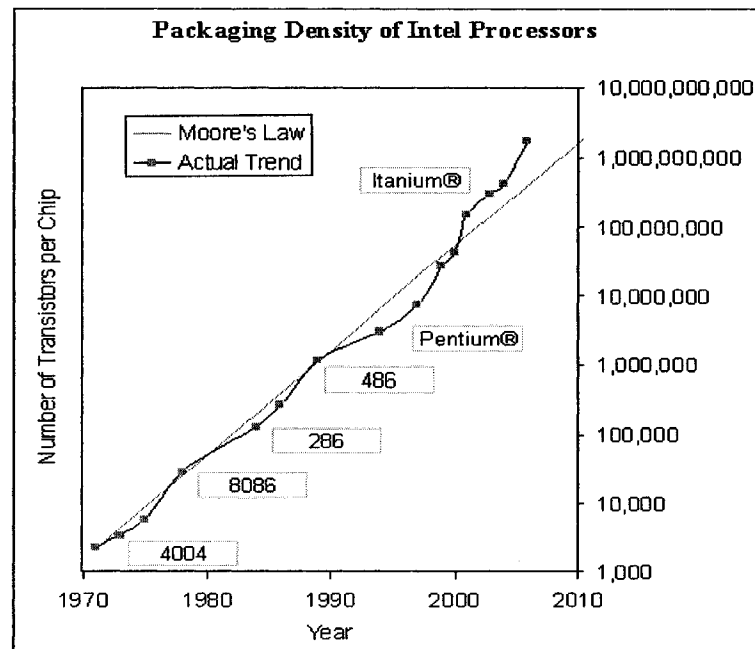
Figure 1.2 Comparison between Moore's law prediction and actual observed trend.

The world's first single chip microprocessor, the Intel 4004 was marketed in 1971. It had 2,250 transistors integrated on a single silicon wafer. Advanced architecture and lithography techniques allowed ultra-high dense packaging of transistors in today's microprocessors. Intel's Montecito processor (belonging to

Itanium 2 processor family, 2006) houses 1.72 billion transistors within a two core die of 596 mm² area [1]. Exposure systems have evolved throughout this period aiming to achieve dense packaging using shorter wavelengths. 'Technology node', also known as 'technology generation' refers to the size of elements on the chip. Figure 1.3 shows that i-line and g-line exposure systems that have dominated over six generations of technology nodes over a period of fifteen years [2]. Deep Ultra-Violet (DUV) lithography has been used up to 130 nm technology node.
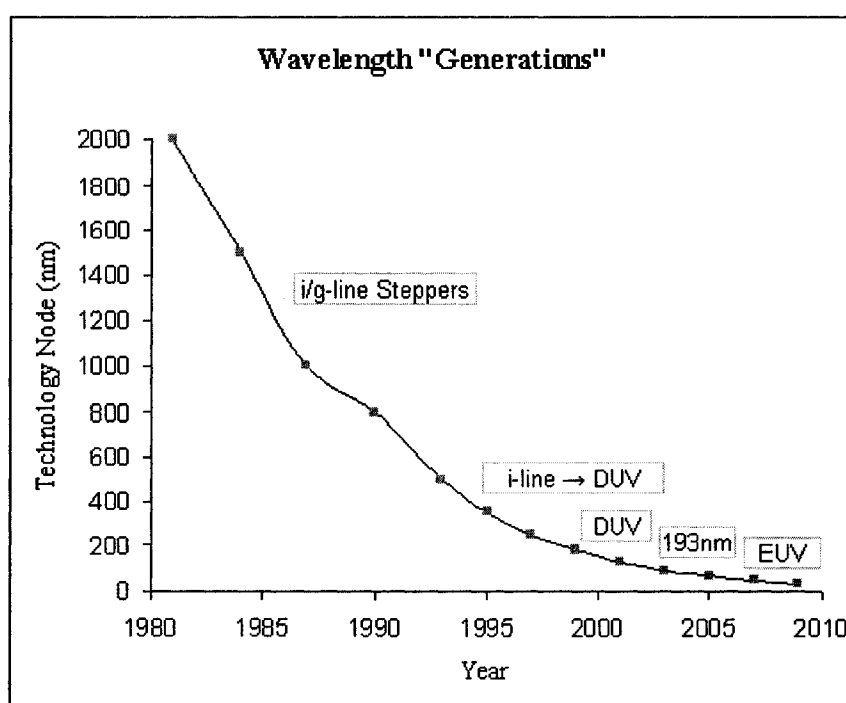
Figure 1.3 Trend of downscaling of semiconductors. Redrawn from reference [2]. Copyright 2002 Intel®.

Immersion lithography is an optical enhancement technique in which a fluid is placed between the light source and surface of the wafer. At 90 and 60 nm technology nodes, 193/157 nm exposure systems with immersion has been dominantly used. The International Technology Roadmap for Semiconductors (ITRS) however, predicts the

requirement of a new generation of exposure systems with even shorter wavelengths at the beginning of the 45 nm node [3]. Extreme Ultra-Violet (EUV) with 13.5 nm wavelength exposure system, also known as Next Generation Lithography (NGL) is capable of meeting the requirements of 32 nm node and lower. However, low throughput, high defect rate and very high power requirement for such an exposure system makes it unsuitable for mass production at this stage. Problems related to mask fabrication process control, metrology and defect inspection, and gate critical dimension control currently prevent NGL from becoming mainstream technology for 45 nm node. Development of advanced lithography systems is costly and increases the manufacturing cost per chip. Hence, research into alternatives to lithography and more cost effective micro-manufacturing techniques should be vigorously pursued.

1.3 Nanotechnology and Nanowires

Nanotechnology, defined as fabrication of devices with atomic or molecular scale precision, is mainly based on 'bottom-up' approach. Devices with minimum feature sizes less than 100 nanometers (nm) are considered to be products of nanotechnology. At these dimensions, quantum effects are expected to play a considerable role in performance of the device. Techniques developed through nanotechnology are expected to address the downscaling issues of present microfabrication technology. Nanotechnology is currently in its infantile stage. However, the ability to organize matter on the atomic scale using scanning Tunneling Microscope (STM) and Atomic Force Microscope (AFM) has been demonstrated. Nanotechnology is projected to find applications in almost all walks of life. Its applications in electronics, medicine, aerospace, surface coating, and cosmetics are being explored. Novel nanomaterials like carbon nanotubes and bucky balls have

been shown to have exceptional tensile strength, and electrical and thermal conductivity. Even though there has been 'hype' in the market for brand names and trademarks containing the word "nano", successful commercial products are still in the early stage of development. Sunscreen lotions containing zinc oxide nanoparticles, stain-free fabrics, and nanocapsules for drug delivery are some of the emerging nano-tech products in the market. There has been a steady increase in total world government investment on nanotechnology since 1997 and even steeper raise since 2002 [4].

Nanowires are one-dimensional nanostructures with diameters typically less than 100 nm. Research on nanowires shows their promising applications as functional components in nanoscale electronic devices. An example of such a device with broad potential for applications is the nanowire Field Effect Transistor (FET). FETs built on silicon [5, 6], germanium [7] and gallium-nitride [8] nanowires have been demonstrated. These nanowire FETs were assembled by complemetry n- and p-type doping on nanowires using metal-catalyzed chemical vapor deposition. Molecular nanowires derived from poly(3-methylthiophene) conducting polymers or organic molecules like 2,2,6,6-tetramethyl-1-piperidinyloxy (TEMPO) self-assembled on to an underlying substrate has been shown to have potential to operate at single-molecule level acting as an interconnects in nanocircuits [9-11]. Such interconnects are expected to have properties similar to a resonance tunneling diodes.

Nanowires are synthesized using three basic methods [12]: 1) Catalyzed growth by Vapor-Liquid-Solid (VLS) mechanism [13]; 2) Template-based electrochemical synthesis [14]; and 3) Solvothermal or wet chemistry [15]. Catalyzed growth by VLS mechanism promotes vertical growth of nanowires on a substrate using three steps: metal

alloying, crystal nucleation, and axial growth. Electrochemical synthesis using nanoporous template, step-edge template, carbon nanotube template, and Deoxyribonucleic Acid (DNA) and polymer template have been synthesize metal and metal oxide nanowire.

1.4 DNA-Templated Nanowires

DNA is being recognized as a nanomaterial and bio-template, in the research field of nanotechnology. Recent research on DNA-templated nanowires, DNA nanoarchitectures, DNA computing and DNA biocatalysts have shown DNA molecule to be one of the most promising functional nanomaterials [16]. Molecular lithography using DNA has demonstrated the ability to transfer pattern with feature size as small as 10 nm [17]. Specific base-pair recognition between complementary DNA single-strands allow them to be used in engineering well-ordered structures at the nano-scale. The inherent addressing capabilities, facilitated by specific interactions between complementary single strands, are manifested in specific recognition and self-assembly processes. In DNA based molecular lithography, the specific DNA sequence is the equivalent of a molecular mask, and the DNA-binding protein serves as the resist (Figure 1.4).
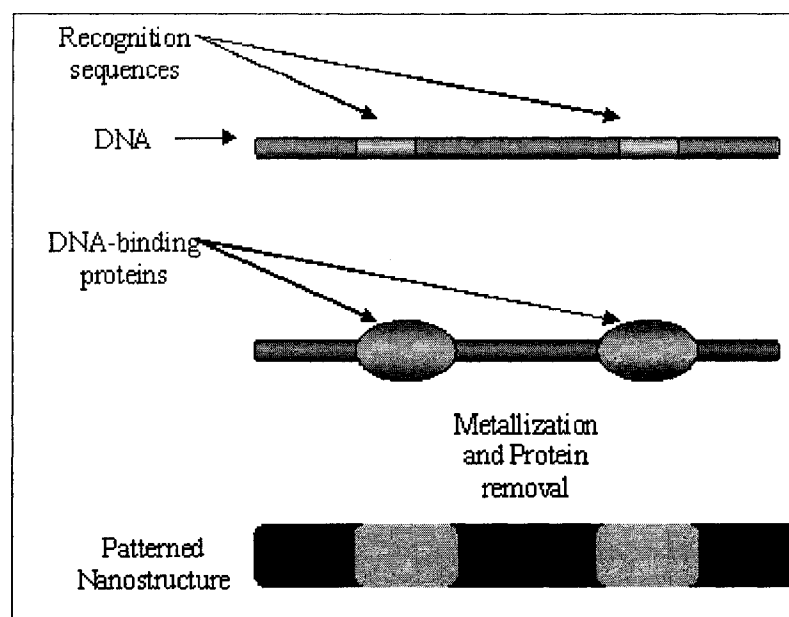
Figure 1.4 DNA molecular lithography using DNA. Redrawn from reference [17].

DNA is a natural template for high aspect ratio (ratio of length of the structure to its diameter) nanostructures. The linear polynucleotide chain has a width of 2 nm and a length of 0.34 nm per nucleoside subunit (Figure 1.5). A wide range of molecular lengths, from nanometres to microns, can be realized with established technology in molecular biology, for example DNA ligation, enzymatic digestion, and polymerase chain reaction. DNA-templated nanowires could be prepared with an almost unlimited range of aspect ratio. A DNA molecule has two classes of binding site: negatively charged phosphate groups and aromatic bases. Figure 1.5 shows a schematic diagram of the structure of double-stranded DNA. The polyanionic backbone of the molecule, composed of alternating sugar and phosphate groups, binds to metal cations or cationic nanoparticles through electrostatic interaction. Various transition metal ions bind to the nitrogen atoms of the DNA bases to form metal–DNA complexes by coordination coupling involving two d-orbitals. For example, the N7 atoms of the bases guanine (G) and adenine (A)

binds strongly with Pt(II) and Pd(II) ions [18] to form complexes, and the N3 atoms of the bases Thymine (T) and Cytosine (C) also strongly interact with Pd(II) ions [19]. Both binding sites have been utilized in nanowire fabrication [20-28]. DNA is uniquely suited to molecular recognition: Specifically A pairs with T, and G with C (Figure 1.5). Loweth *et al* [29] have used this so-called Watson–Crick base pairing to assemble two or three individual Au nanocrystals on specific sites of single-stranded DNA (ssDNA) molecules. DNA-templated metallic nanowires tend to have different structural properties compared with semiconductor nanowires fabricated by various approaches (latter discussed in Chapter 4), because metal nanoparticle arrays on DNA prepared by wet chemistry lack crystallinity and uniformity [20-25].

To control the orientation and length of the DNA-templated nanowires in the required position inside the device, the DNA molecules need to be manipulated on the surface before further processing. Individual DNA molecules must be synthesized with specific number of base pairs, separated, and stretched on a substrate to serve as templates for nanowire fabrication. The number of base pairs and the stretching process will determine the length of DNA template and the nanowire formed. In addition, appropriate 'interfacing' of DNA with conductive elements using chemical modification or adjustment of conditions will be required to connect the DNA-templated nanowires to devices in a nanoscale electronic circuit. Interconnection can be realized by a number of different approaches to the specific coupling of DNA to a conductive surface. Therefore, advanced manipulation of DNA before the metallization process can be important for the precise positioning of nanowires.
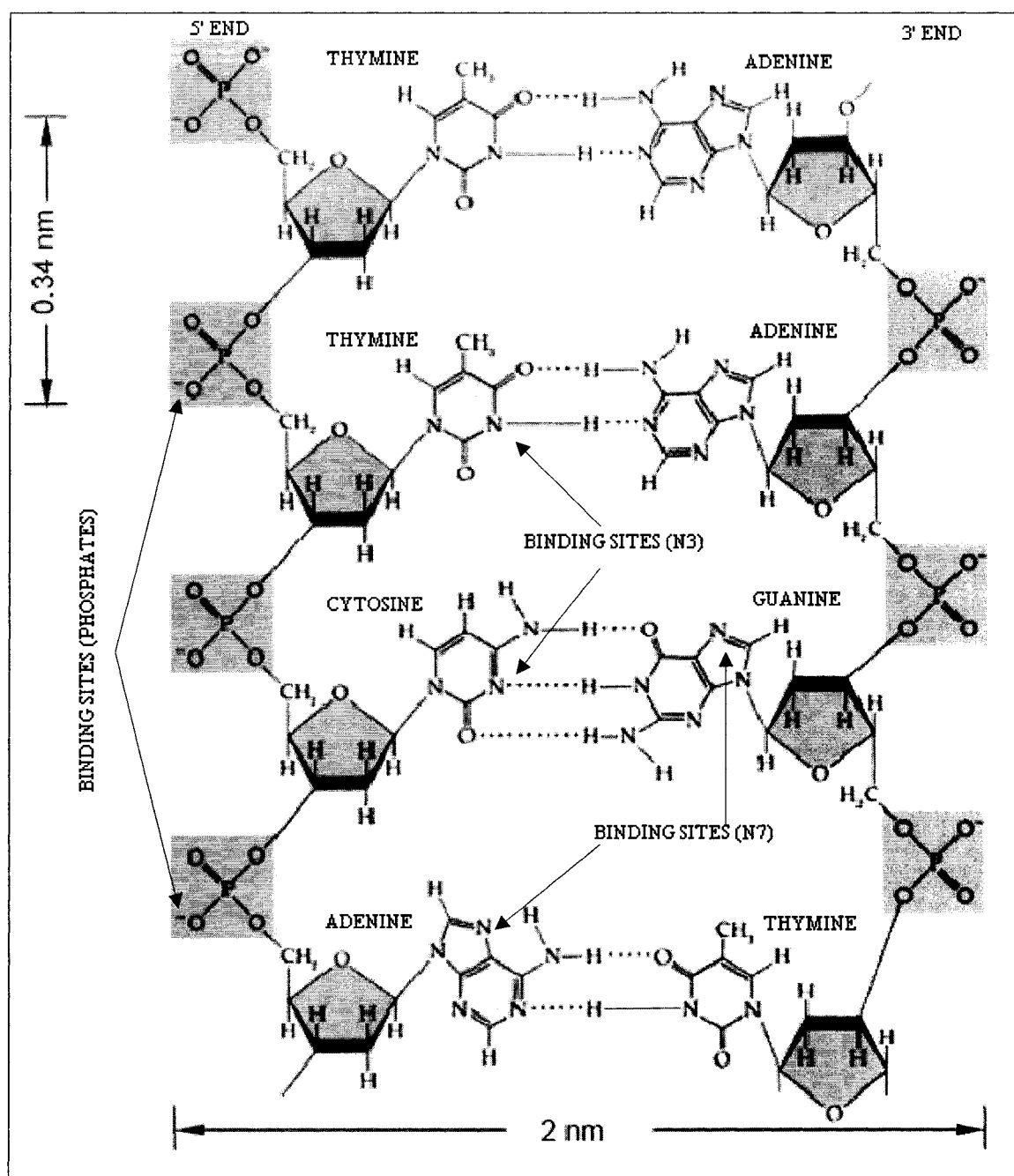
Figure 1.5 Schematic diagram of the structure of double-stranded DNA. Two classes of binding site for DNA-templated metallic nanowire fabrication are shown: negatively charged phosphate groups in the polymer backbone, and N7 atoms of bases G and A and N3 atoms of bases C and T.

The metal nanostructures in DNA-templated platinum, palladium and silver nanowires prepared by metallization of DNA have a heterogeneous crystal structure and high degree of roughness [20-25]. As a result of structural defects, these nanowires exhibit only a fraction of electrical conductivity of the bulk metal. The two common sources of high and non-linear resistance of DNA-metallized nanowires are non-ideality of nanowire shape [20] and inter-grain boundaries [20, 30]. It is reported [31, 32] that electrical conductivity of metal structures with defects can be enhanced through heat treatment. It has been observed [23] that annealing metallized nanowires assembled on single DNA molecules by chemical deposition of a thin continuous palladium film, reduces the resistance by up to a factor of four. Indium has a considerably low melting point of 156.60 °C as compared with other metals (silver m.p. 961.78 °C; gold, m.p. 1064.18 °C; copper, m.p. 1084.62 °C; palladium, m.p. 1554.9 °C; platinum, m.p. 1768.3 °C) used for DNA-templated nanowire assembly. The lower melting point facilitates the heat treatment of indium nanowires assembled in nanocircuits without damaging the substrate and other components. However, the electrical resistivity of indium (83.7 $n\Omega \cdot m$, at 20 °C) is five times higher than that of the most common conductor copper (16.78 $n\Omega \cdot m$, at 20 °C). DNA-templated silver nanowires have been observed [20] to exhibit ohmic behavior. Electrical resistance of a 16 μm silver nanowire was measured [20] to be 7 M Ω, which is much higher compared to bulk silver (0.2544 Ω for 16 μm of bulk silver, assuming resistivity of bulk silver as 1.59 x 10^{-8} Ω m). This difference in resistivity implies that heat treated DNA-templated indium nanowires could exhibit resistivity close to bulk indium and can have electrictical conductivity values higher than other DNA-templated metal nanowires.

CHAPTER 2

PRECURSORS TO DNA TEMPLATED NANOWIRES

2.1 Introduction

DNA-templated metal nanowires have been fabricated using various kinds of metal salts and complexes. Acetate salts of palladium [30] and platinum [26] have been used as precursors in assembly of nanowires on DNA templates. DNA-templated copper nanowires [33] and silver nanowires [34] have also been synthesized from copper sulfate and silver nitrate, respectively. Indium(I) salts are highly unstable and tend to dispropotionate to indium(II) and indium(III); however, it is possible to stabilize indium(I) by incorporating the indium ion into a stable organic indium coordination complex. We have synthesized a stable indium(I) complex as a precursor for fabricating DNA-templated indium nanowires.

2.2 Synthesis of [(Hydroboratotris(3'-phenylpyrazolyl))indium

2.2.1 Literature Review

2.2.1.1 Metal Complex Chemistry

A metal or coordinated metal complex is a product of a Lewis acid-base reaction in which neutral molecules or anions (called ligands) bond to a central metal atom (or ion) by coordinate covalent bonds. A ligand is an atom, ion, or a molecule that generally donates one or more of its electron pairs to form a coordinate covalent bond that shares

14

its electrons through a covalent bond with one or more central metal atoms [35]. In an organometallic coordination complex, the metal atom coordinates with one or more carbon atoms of the ligand. The properties of coordinated metal compounds, whether in classical inorganic coordination complexes or in organometallic compounds, are determined in large measure by the type of atoms coordinating to the metal and the steric factors [36].

2.2.1.2 Indium Complexes

Metal complexes have been synthesized by the reactions of ligands with the metal salts or metal carbonyls. This method is also known as immediate (direct) interaction of ligands and sources of metal centers [37]. Synthesis of several types of indium complexes of indium(I), (II) and (III), synthesized using this method have been reported so far. In 1966, Goggin et al. [38] reported the synthesis of aniline and morpholine complex of indium(I) and indium(II) using indium mono, di-halides and morpholine solutions in diethylether. However, these complexes were found to be very unstable. Trivalent indium(III) complexes of thiocyanate [39], phospholyl [40], dithiocarboxylates [41], tricyclopentadienyl [42], dihydrobis(3,5-dimethylpyrazolyl)borate [43], tripodal iminophenolate ligand [44] and tridentate, substituted pyrrole ligand [45] have also been successfully synthesized and characterized.

Synthesis of monovalent indium(I) complexes has been a significant challenge due to extreme sensitivity of indium(I) towards air and moisture. Common synthetic routes [46] to indium(I) compounds with indium in the formal oxidation state of +1 are: 1) substitution of weakly bonded ligands like CO and ligands of the type InR (R=e.g. pentamethylcyclopentadiene (Cp*), $C(SiMe_3)_3$, $Si(t\text{-}Bu)_3$ or sterically hindering aryl

groups); and 2) salt elimination and insertion reactions. Of these, ligands that exibit multihapto (group of contiguous atoms of the ligand are coordinated to a central metal atom simultaneously) coordination have gained popularity in nanoparticle synthesis. Steric repulsion between ligands is necessary to prevent aggregation into complexes with higher coordinated metal centers [47] and increase the stability of the metal ions. Organometallic indium complexes based on π-systems can be classified into two general classes, η^5-cyclopentadienyl and η^6-arene-type derivatives [48].

2.2.1.2.1 Cyclopentadienyl Derivatives

The first η^5-cyclopentadienyl indium complex to be reported [49] was η^5-(cyclopentadienyl)indium (η^5-In(C$_5$H$_5$)). The synthesis route for η^5-In(C$_5$H$_5$) was latter modified [50]. η^5-In(C$_5$H$_5$) was synthesized from Li(C$_5$H$_5$). Li(C$_5$H$_5$) and InCl were stirred in ether under vacuum at room temperature for 17 h. Ether was removed by vacuum distillation and η^5-In(C$_5$H$_5$) was recovered by sublimation under vacuum at 55 °C. X-ray diffraction studies suggested a zigzag polymeric chain of In(η^5-C$_5$H$_5$) units in the solid state [48]. A similar compound, η^5- (Monomethylcyclopentadieny)indium(I) (η^5-In(C$_5$H$_4$Me)) has also been synthesized [48] using method analogous to synthesis of η^5-In(C$_5$H$_5$). Both η^5-In(C$_5$H$_5$) and η^5-In(C$_5$H$_4$Me) are highly sensitive to oxygen and moisture making it difficult to be synthesized and characterized. An isotropic atomic vibration ellipsoids for crystallographic asymmetric units of In(C$_5$H$_5$) and In(C$_5$H$_4$Me) are shown in Figure 2.1. The geometry of these complexes disallows complete encapsulation of the indium ions, making them prone to decomposition.
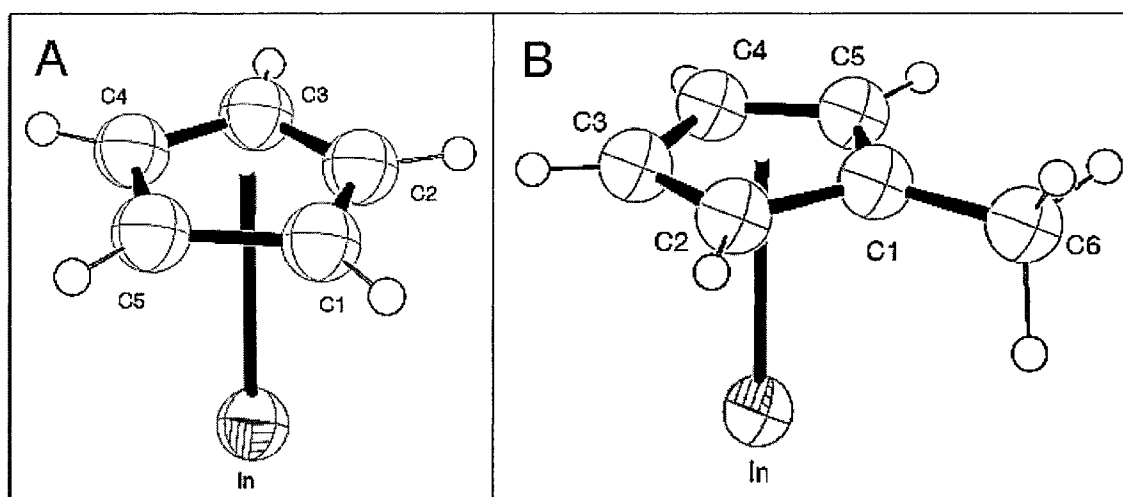
Figure 2.1 Labeling of atoms and isotropic atomic vibration ellipsoids for crystallographic asymmetric units. A) η^5-In(C_5H_5). B) η^5-In(C_5H_4Me). Redrawn after reference [48].

2.2.1.2.2 Pyrazolyl Derivatives

Non π-system or non arene-type ligands such as poly(pyrazolyl)borates are based on complex arrangement of coordinating atoms, exhibiting steric factors protecting the metal center. The poly(pyrazolyl)borate family of ligands, were first reported [51] by Trofimenko in the 1966. These mono-anionic ligands have facially coordinating N-donors that can exibit polydenticity (coordination *via* multiple coordination sites within the ligand) [52]. The steric factor around the metal center can be altered by changing the substituents on the pyrazolyl rings of the ligands [43]. The coordination chemistry of poly(pyrazolyl)borates has been reviewed [53] extensively.

Prompted by the formal analogy between cyclopentadienyl anion and HB(pz*)₃ (where pz* is 3,5-dimethylpyrazole), [bis{(3,5-dimethylpyrazolyl)₃hydridoborato}In]I was synthesized [54]. It was observed [43] that, slow increase of the temperature of the reactants from -30 °C to ambient temperature caused gradual disproportionation of In(I) to In(III) and In(0) in the presence of HB(pz*)⁻. It was hypothesised [55] that use of a

more sterically hindered pyrazole than pz* might facilitate the isolation of a stable In(I) species. As the 3, 4 and 5 positions of the pyrazole ring are made available for substitution, it is possible to synthesize [51] pyrazole ligand with N3 positions substituted by bulky groups such as isopropyl [56], tert-butyl [57] or phenyl [55], enhancing its steric hindrance to make these complexes more stable.

An air-stable monomeric indium(I) complex, [(hydroboratotris(3'-phenylpyrazolyl))indium] have been synthesized [55] by reacting indium iodide with HB(3-pz**)$_3^-$ (where pz** is 3-phenylpyrazol) in tetrahydrofuron at -50 °C. The structure [55] of [(hydroboratotris(3'-phenylpyrazolyl))indium] is shown in Figure 2.2. Here, indium adopts a pyramidal geometry with respect to the coordinated nitrogen atoms. It has also been deduced [55] that there is no In-In interaction in this compound in solid-state, making it accessible for further reactions.
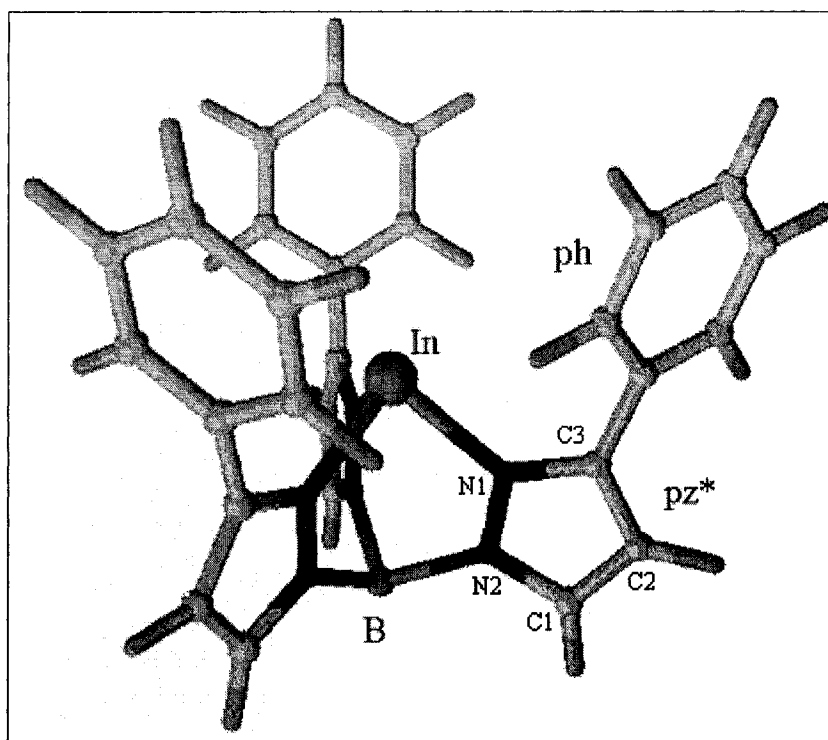
Figure 2.2 Structure of hydroboratotri(3-phenylpyrazolyl)indium with atom-labeling scheme. Redrawn after reference [55].

2.2.2 Synthetic Strategy

Pyrazol (also known as 1,2-Diazole, abbreviated as -pz) is a simple aromatic ring organic compound of the heterocyclic series characterized by a 5-membered ring structure composed of three carbon atoms and two nitrogen atoms in adjacent positions. They are synthesized through the reaction of α,β-unsaturated aldehydes with hydrazine and subsequent dehydrogenation. The structure of pyrzol is shown in Figure 2.3A. A phenyl group (also known as phenyl ring, abbreviated as -ph) is a functional group with the formula C_6H_5. Ph has a cyclic ring structure with six carbon atoms. The structure of phenyl group is shown in Figure 2.3B.
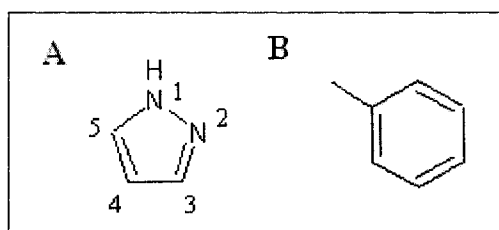
Figure 2.3 Structural formula of functional groups. A) Pyrazol B) Phenyl.

It has been found [58] that in 3-substituted pyrazoles, alkyl groups prefer to occupy position 5 next to NH, while aryl groups seem to prefer position 3 next to N. Hence, in 3-phenylpyrazol, the phenyl group occupies the 3 position in pyrazol. 3-phenylpyrazol is synthesized by substituting the hydrogen in position 3 by a phenyl group. Figure 2.4 gives the equations outlining the reactions involved during the synthesis of 3-phenylpyrazol.
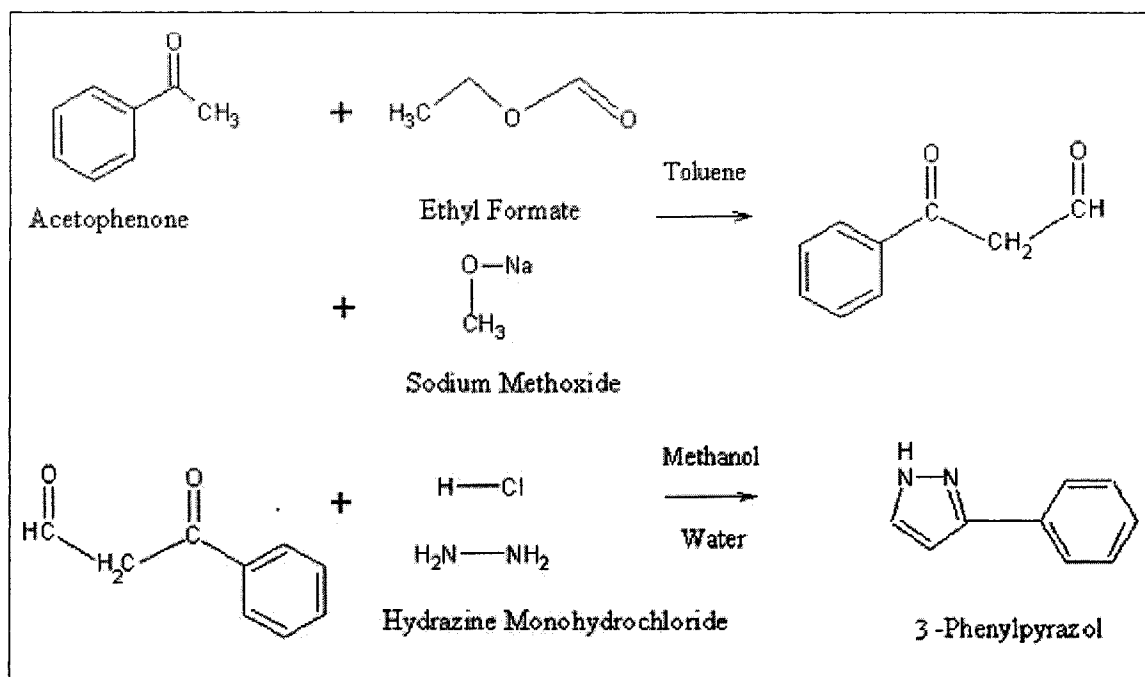
Figure 2.4 Schematic chemical equations for synthesis of 3-Phenylpyrazol

Synthesis route for [HB(3-phenylpyrazol)$_3$]In form 3-phenylpyrazol involves 3 steps as shown in chemical equations listed in Figure 2.5. In the first step, potassiumdihydrobis(3-phenylpyrazol-1-yl)borate ([KH$_2$B(3-phpz)$_2$]) is synthesized from 3-phenylpyrazol and potassium tetrahydroborate. The second step involves addition of another 3-phpz group to ([KH$_2$B(3-phpz)$_2$], giving [KHB(3-phpz)$_3$]. In the third step, KHB(3-phpz)$_3$ reacts with InCl to yield [HB(3-phpz)$_3$]In.
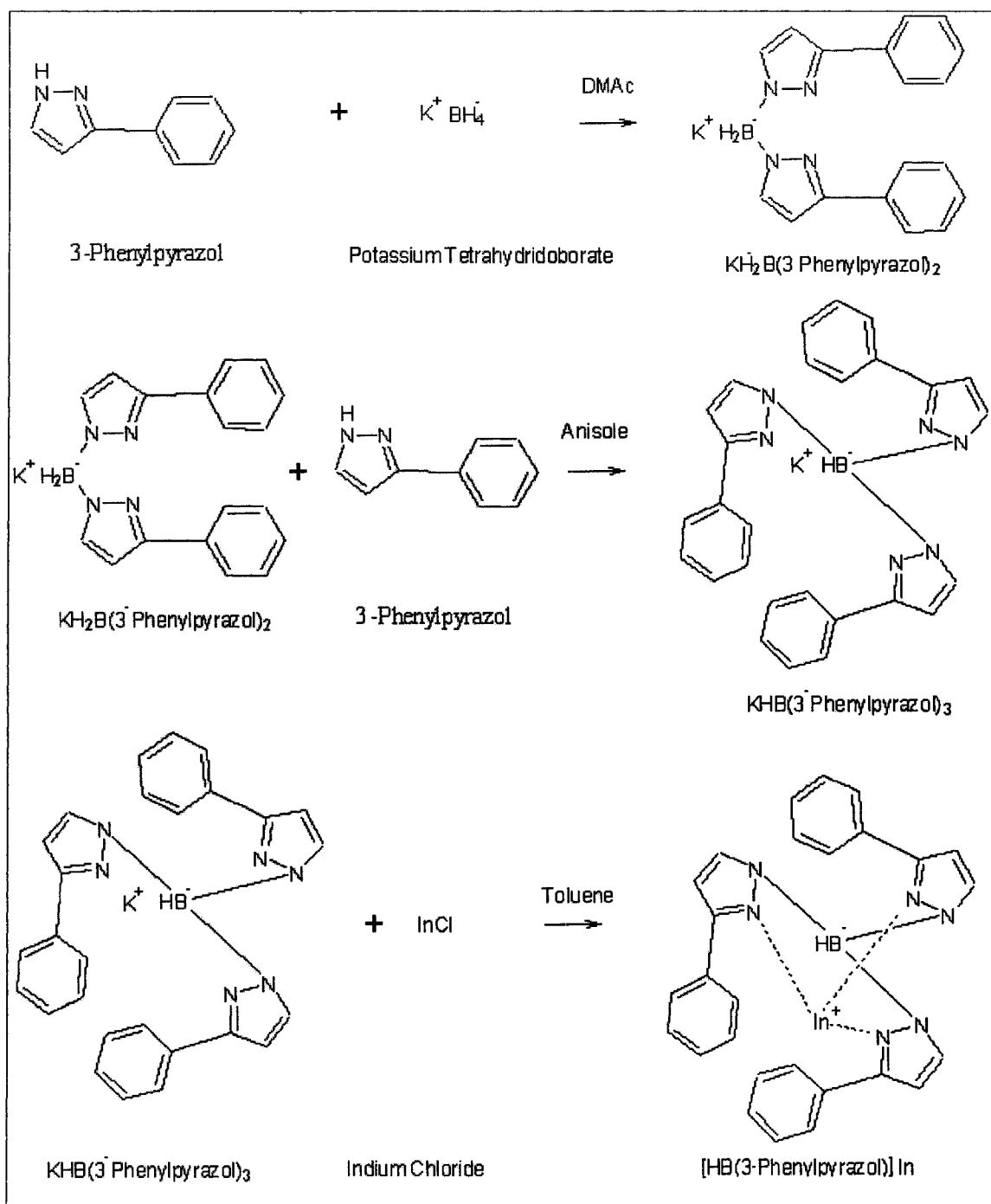
Figure 2.5 Schematic chemical equations for synthesis of [HB(3-phpz)₃]In

2.2.3 Materials

All chemicals used in the synthesis were reagent grade and were used as received. Acetophenone (99% pure), Methanol (98% pure), Potassium Tetrahydroborate (powder, 98% pure) and Indium (I) Chloride (InCl) (anhydrous, 99.995%) were ordered from Alfa Aesar. Ethyl Formate (97% pure), N, N-Dimethylacetamide (DMAc) (99% pure), methoxybenzene (Anisole) (98% pure), Toluene (99.8% pure), Sodium Methoxide (powder, 95% pure) and Hydrazine Monohydrocholoride (powder, 98% pure) were from Sigma-Aldrich. Dichloromethane (98% pure), Hexane (98% pure) and Tetrahydrofluoron (THF) (stabilized by 250 ppm BHT, 99.7% pure) were from EM-Science. NMR solvents used were spectroscopic grade. Chloroform-d (99.6% atom %D) and Acetone-d$_6$ (99.7% %D) were from Sigma-Aldrich. Toluene was dried by refluxing under nitrogen with calcium hydride (10 mg per mL) for over 24 h (detailed procedure listed in appendix) and then was distilled using the vacuum line (Figure 2.6). It was then degassed using 3 cycles of freeze-pump-thaw procedure [59] (detailed procedure listed in section B of the appendix). THF was first distilled using vacuum line and then dried by refluxing under nitrogen with sodium and benzophenone till the solution turned dark purple color (~24 h). THF was then used after subsequent distillation and degassing.

2.2.4 Experimental Techniques

A vacuum line equipped with Welch® DuoSeal® vacuum pump and silicone-oil diffusion pump was used for all distillation, degassing and solvent transfer processes. Working pressure was less than 10^{-5} mm Hg. The pressure was monitored using a calibrated Varian® Thermocouple (TC) pressure gauge as well as a McLeod gauge. Liquid nitrogen traps were used at various stages to prevent volatile solvents from

entering into the oil diffusion pump. A schematic sketch and a photograph of the vacuum line used is shown in Figure 2.6. A slurry prepared by mixing chlorobenzene and liquid nitrogen in flask was used for maintaining a temperature of -50 °C wherever required. InCl is a highly air-sensitive compound. Hence, it was stored and manipulated inside a nitrogen atmosphere VAC® dry-box equipped with PEDATROL pressure control system (Figure 2.7) and was prepared freshly grounded before use. All glassware were thoroughly cleaned with KOH/alchol, washed thoroughly, air dried and oven dried (> 4 h).
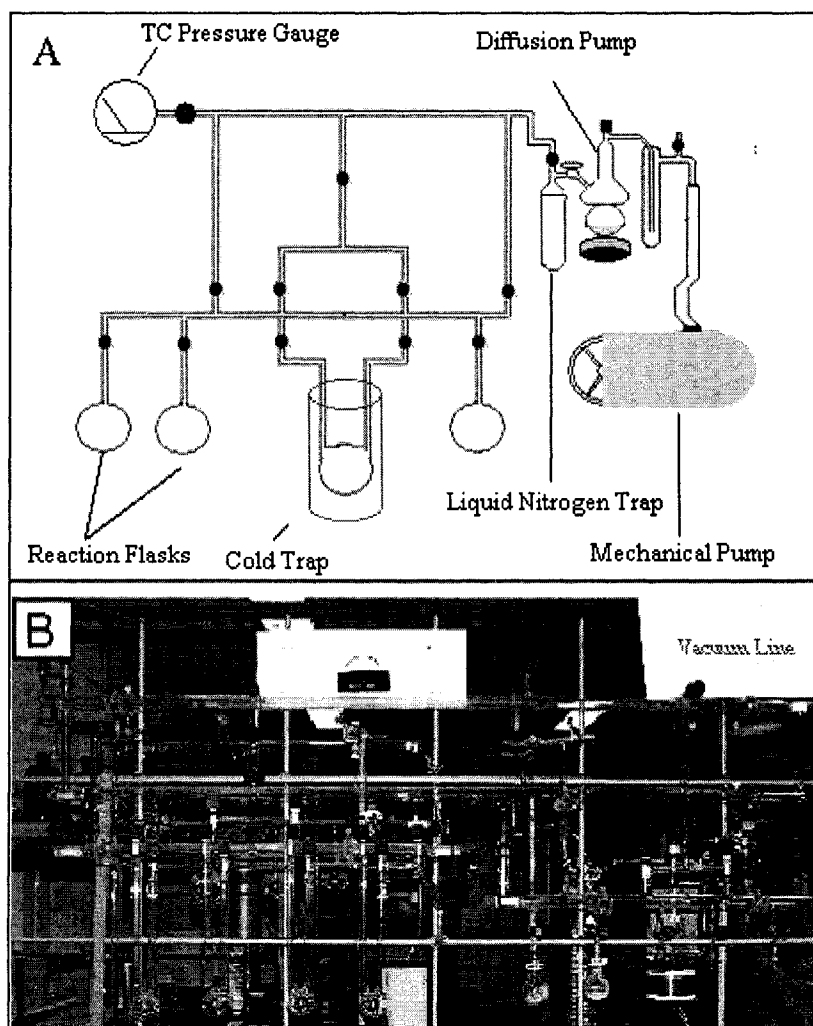
Figure 2.6 Vacuum line setup. A) Schematic sketch. B) Photograph.
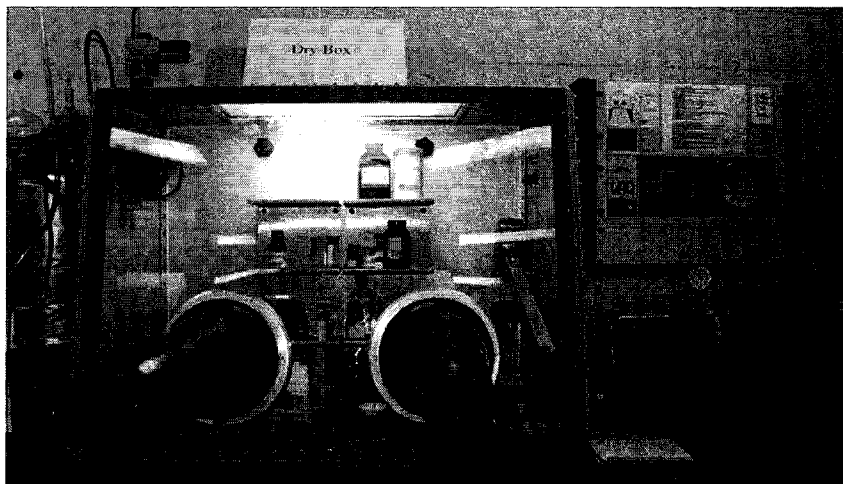
Figure 2.7 Photograph of nitrogen atmosphere Dry-Box

General reactions (reactions not critical to air and moisture) were performed in beakers of suitable volumes over Corning® PC-351 Hot Plate-Stirrer (Figure 2.8A). Reactions requiring refluxing were setup such that evolving gases will pass through a water cooled condenser and bubble out of a mercury trap (Figure 2.8B). All setups were properly clamped under a Supreme Air LV (Kewaunee® Scientific Corporation, USA) fume hood. Reactions involving distillation/sublimation of the product or stripping of solvents were performed in a round-bottom flask of suitable volume connected to a distillation trap assembly (Figure 2.8C). The reaction temperature was maintained using a heated oil bath, heating mantle controlled by J-KEM® Digital Temperature Controller (Model 260/Timer) or dewar flask filled with slurry of chlorobenzene and liquid nitrogen at -50 °C. The connecting tube was wound with a heating coil to avoid condensation of products in the tube. Filtration and washing of precipitates were performed using either Buchner funnel and Whatman® filter paper (fine grade, 1 μm porosity) apparatus or

Hirsch funnel (fine grade, 1 μm porosity) with a filter flask connected to a water

aspirator. Figure 2.8D shows the apparatus used for filtering and washing. A 250 mL

separatory funnel was used for all solution extraction procedures. Nuclear Magnetic

Resonance (NMR) spectra were obtained with a JEOL® JNM-GSX 270 FT NMR system.

3-4 cm long NMR samples were prepared in 5 mm thin-wall NMR tubes. NMR data for

^{1}H, ^{13}C-decouple and ^{13}C-couple isotopes were collected after 150, 1000 and 3000 scans

respectively.
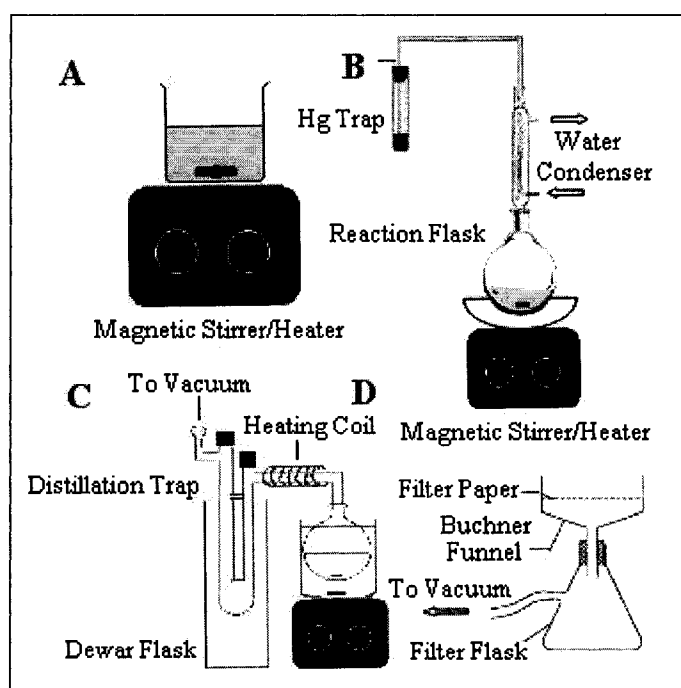
Figure 2.8 Experimental setup for synthesis. A) General reaction. B) Reflux reaction. C) Vacuum distillation. D) Filtering and washing.

2.2.5 Synthetic Procedures

Synthesis of [HB(3-phpz)₃]In involved 4 stages. The first three stages each

yielded a stable compound used in subsequent stages as the starting material. Yield from

more than one trial of each stage were combined. Air-stable [HB(3-phpz)₃]In was

obtained in the final stage. 3-Phenylpyrazol was synthesized in the first stage. The procedure outline for synthesis of 3-Phenylpyrazol was from reference [60]. 3-Phenylpyrazol was reacted with potassium tetrahydridoborate in the second stage to obtain $KH_2B(3\text{-phpz})_2$. The third and fourth stage of synthesis procedure yielded KHB(3-phpz)$_3$ and [HB(3-phpz)$_3$]In respectively. The procedure outlined for synthesis of $KH_2B(3\text{-phpz})_2$ and KHB(3-phpz)$_3$ has been reported [57]. The synthesis route for [(HB(3-phpz)$_3$)$_2$In] from InI has been demonstrated previously [54]. The synthesis procedure [HB(3-phpz)$_3$]In from InCl has been derived from Ref [54]. The quantities of reactants, temperatures and other miscellaneous parameters have been suitably modified to obtain better yield and purity and to adapt to available equipments.

2.2.5.1 Synthesis of 3-Phenylpyrazol

a) A slurry of sodium methoxide (10.8 g, 0.2 mol) in 150 mL of toluene is prepared in a 400 mL beaker. Gentle heating and rapid stirring was used.

b) Acetophenone (23.366 g, 0.20mol) and ethyl formate (22.2 g, 0.30 mol) were added to the slurry in one portion. Vigorous reaction takes place and solid precipitate starts forming.

c) After stirring for 1 h, the solid is filtered and washed with hot toluene and hexane to remove excess reactants. Filtrate was thoroughly air-dried (30 min – 1 h). Solid was slurried in methanol (100 mL) by stirring and gentle heating.

d) Hydrazine monohydrochloride (13.7 g, 0.20mol) was dissolved in water (100 mL) and added to the methanol slurry along with stirring. The reaction was allowed to continue for 2 h with slight heating (~50 °C).

e) Products were extracted with dichloromethane (100 mL). The solvent was stripped from the extract using vacuum distillation. The product was then purified further by distillation (boiling point 139 °C (0.9 mm Hg)).

2.2.5.2 Synthesis of KH$_2$B(3-phpz)$_2$

a) 3-Phenylpyrazol (3.17 g, 0.022 mol) condensed in the distillation trap was dissolved in N,N-dimethylacetamide (DMAc) (100 mL) by gentle heating and poured in a 200 mL beaker.

b) Potassium tetrahydridoborate (0.54 g, 0.01 mol) was added along with stirring.

c) The solution was transferred to a 250 mL round bottom flask and was setup under the fume hood after attaching the water condenser and mercury trap. The flask was stirred and heated to mild boiling so that hydrogen gas bubbling through mercury trap is visible. The reaction was allowed to continue till hydrogen evolution ceased (~ 12h).

d) All volatile solvents were removed under high vacuum by heating at 130 °C.

e) Part of the product was purified by recrystallization using THF. The purified product was used for characterization. The crude product was used in the next stage.

2.2.5.3 Synthesis of KHB(3-phpz)$_3$

a) KH$_2$B(3-phpz)$_2$ (3.78 g, 0.011 mol) was dissolved in anisole (80 mL) in a 150 mL beaker. 3-phenylpyrazol (1.6 g, 0.11 mol) was added along with stirring.

b) The solution was transferred to a 250 mL round bottom flask and refluxed with vigorous stirring for 12 h. Hydrogen gas should bubble through the Hg trap.

c) The reaction mixture was cooled, filtered, washed with hot toluene and then with hexane, and air-dried (30 min-1 h).

d) The product was purified by recrystallization using THF.

2.2.5.4 Synthesis of [HB(3-phpz)₃]In

a) InCl (0.375 g, 0.025 mol) was added to KHB(3-phpz)₃ (2.42 g, 0.005 mol) in a Schlenk vessel in a dry box. The Schlenk vessel was closed and evacuated by connecting to the vacuum line. The reactant mixture was cooled to -50 °C using chlorobenzene and liquid nitrogen slurry.

b) Dry degassed toluene was transferred to the reactant mixture by distillation. The solvent transferred was sufficient to submerge the reactants. The mixture was stirred overnight (~ 12 h) and the temperature was allowed to slowly raise from -50 C to room temperature.

c) The color of the solution should change from faint gray-white to dark gray as the temperature is raised.

d) The solution was filtered and the toluene filtrate was collected.

e) The residue was washed with dry THF. Solvents from toluene filtrate and THF washings were evaporated under vacuum.

f) Recrystallization and slow evaporation of THF washing should yield white crystals.

2.2.6 Observations and Results

2.2.6.1 3-Phenylpyrazol

Reaction of sodium methoxide with acetophenone and ethylformate was exothermic and accompanied by a change of solution color from milky white to bright

orange. Precipitation of solids began within 30 seconds. Upon adding hydrazine monohydrochloride to the filtered precipitate, the solution turned into bright yellow-green from a milky light-brown color. The product was extracted using dichloromethane. The extraction was performed 3 times and the extracts were combined. Solvent stripping was initially carried out with a water aspirator. It was later determined that the vacuum line can be used for this process with proper setup. The crude product had a bright yellow-green color. Distillation of the crude product was done at 139 °C under vacuum. 3-Phenylpyrazol was distilled and weighed in the distillation trap while temperature was controlled using a digital temperature controller.

Percent yield for 3 different trials with minor setup changes is listed in Table 2.1. ^{1}H and ^{13}C NMR spectra for 3-Phenylpyrazol is attached in section C of the appendix (Figure 1-3) and a summary of the peaks has been listed in Table 2.2. ^{1}H NMR peak at 7.34 ppm and ^{13}C NMR peak at 128.45 ppm, confirmed the presence of phenyl group. ^{1}H NMR peak at 7.74 ppm and 6.60 and ^{13}C NMR peak at 104.09 and 127.65 ppm confirmed the presence of pyrazole group.

Table 2.1 Yield results for 3-phenylpyrazol.

Trial Number	Remarks	Theoritical Yield (mmols)	Measured Yield (mmols)	Percent Yield (%)
1	Water aspirator used for stripping solvent, no heating used in reactions.	207.0	123.9	59.9
2	Water aspirator used for stripping solvent, Gentle heating used during both reactions.	198.0	131.7	66.5
3	Vacuum line used for stripping solvent, Gentle heating used during both reactions.	204.0	135.5	66.4

Table 2.2 NMR results for 3-phenylpyrazol.

NMR	Peak Numbers, δ (ppm)
^{1}H	2.14, 2.33, 6.60, 7.32, 7.34, 7.36, 7.39, 7.42, 7.59, 7.74, 7.77
^{13}C-Coupled	76.68, 77.15, 77.63, 101.37, 103.95, 104.09, 124.76, 127.65
^{13}C-Decoupled	76.68, 77.15, 77.62, 102.73, 125.95, 126.72, 128.13, 128.45, 128.88

2.2.6.2 KH$_2$B(3-phpz)$_2$

Potassium tetrahydridoborate and 3-phenylpyrazol were mixed with DMAc in a beaker. Large lumps of potassium tetrahydridoborate were initially formed in the solution. Rapid stirring accompanied by gentle heating was required to obtain a homogenous suspension. This reaction should be set up such that the fluid level does not exceed 50% of the total flask volume to avoid bubbling. A higher level of solvent also makes it difficult to strip the solvent from the product using vacuum later. Temperature should be carefully controlled so that the solution boils moderately. Excess heat should be avoided to prevent decomposition of the compound. Evaporation of the solution after completion of the reaction yielded an amorphous white solid deposited on the walls of the round bottom flask. The product was then dissolved in anisole and stored.

The yields for three different trials of this experiment were comparable and had an average yield of 53.4%. ^{1}H and ^{13}C NMR spectra for KH$_2$B(3-phpz)$_2$ is attached in section C of the appendix (Figure 4-6) and a summary of the peaks has been listed in

Table 2.3. NMR results for KH$_2$B(3-phpz)$_2$ indicated the presence of two 3-phenylpyrazol groups in the compound.

Table 2.3. NMR results for KH$_2$B(3-phpz)$_2$.

NMR	Peak Numbers, δ (ppm)
^{1}H	0.01, 2.02, 2.03, 2.04, 2.05, 2.06, 2.07, 2.32, 2.82, 2.92, 2.98, 3.61, 6.48, 6.68, 7.28, 7.31, 7.36, 7.39, 7.69, 7.83
^{13}C-Coupled	28.23, 28.52, 28.79, 29.37, 29.65, 29.94, 30.26, 205.73, 205.99
^{13}C-Decoupled	28.20, 28.49, 28.70, 29.06, 29.34, 29.63, 29.91, 125.25, 125.37, 126.17, 128.25, 128.63, 205.66, 205.93

2.2.6.3 KHB(3-phpz)$_3$

Anisole solution of 3-phenylpyrazol was mixed with anisole solution of KH$_2$B(3-phpz)$_2$ in one portion in a 250 mL round-bottom flask. The solutions were miscible. After ~4 h of refluxing the reactants, solution started turning clear and white precipitates were formed. The reaction continued for ~12 h, after which evolution of hydrogen stopped. White needle like crystals were obtained after the solution was filtered and the precipitates were washed with hot toluene and hexane. The product was further purified by recrystallization using THF.

Crystals of KHB(3-phpz)$_3$ were air dried and stored (Figure 2.9A). Average percent yield was relatively high for this experiment (67.2 %). ^{1}H and ^{13}C NMR spectra for KHB(3-phpz)$_3$ is attached in section C of the appendix (Figure 7-9) and a summary

of the peaks has been listed in Table 2.4. NMR results were coherent with the presence of three 3-phenylpyrazol groups.

Table 2.4 NMR results for KHB(3-phpz)$_3$.

NMR	Peak Numbers, δ (ppm)
^{1}H	0.00, 2.02, 2.03, 2.04, 2.05, 2.06, 2.07, 2.08, 6.46, 6.48, 7.14, 7.25, 7.28, 7.68, 7.82, 7.
^{13}C-Coupled	28.21, 28.38, 28.49, 29.78, 29.07, 29.34, 29.63, 29.92, 30.24, 30.92, 205.37, 205.66, 205.75
^{13}C-Decoupled	0.0, 28.18, 28.46, 28.75, 29.04, 29.32, 29.61, 29.89, 100.61, 125.32, 126.10, 128.22, 135.16, 205.60, 205.75

2.2.6.4 [HB(3-phpz)$_3$]In

This experiment was repeated four times with ~ 0.005 mol of starting material (KHB(3-phpz)$_3$). All values listed are an average for these four trials. The reaction started after the solvent (toluene) was transferred to the reaction flask containing KHB(3-phpz)$_3$ and InCl. The initial temperature of chlorobenzene-liquid nitrogen slurry was 46.7 °C. The temperature was allowed to rise as the reaction progressed. Temperature change rate was measured to be ~5.5 °C. The reactants were inspected at intervals of 2 h. The color of the reactants darkened as the reaction progressed. Room temperature was reached within a period of ~14 h. Filtering and washing the solution without exposing it to the atmosphere involved a complex procedure. The procedure involved two steps. In

the first, toluene was filtered out. A Reaction flask was connected to a storage flask through a double-ended filter. The assembly was evacuated by connecting to the vacuum line. Toluene was transferred to the storage flask by maintaining a temperature difference between two chambers. In the second step, the precipitates were washed with THF and THF washings collected. The double-ended filter was connected to a flask containing THF and an empty flask was connected to the second end of the filter after disconnecting the reaction flask. The assembly was evacuated and THF was transferred through the residue on the filter into the collection flask.

THF was then evaporated under vacuum to obtain white crystals of [HB(3-phpz)$_3$]In (Figure 2.9B). EDX results for sample recrystallized on silicon substrate suggest an indium composition of ~10% by weight in the compound. ^{1}H and ^{13}C NMR spectra for [HB(3-phpz)$_3$]In is attached in section C of the appendix (Figure 10-12) and a summary of the peaks has been listed in Table 2.5. ^{1}H and ^{13}C NMR spectra for the compound in Acetone-d6 was similar to that of KHB(3-phpz)$_3$.
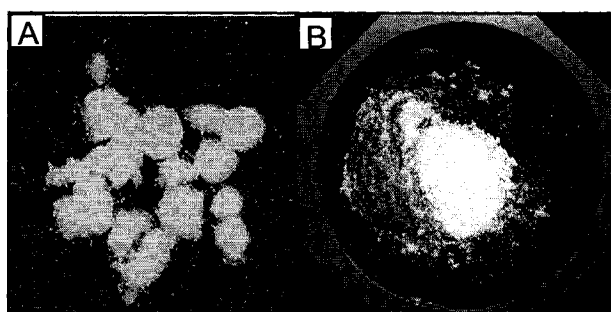
Figure 2.9 Appearance of the synthesized products. A) KHB(3-phpz)$_3$. B) [HB(3-phpz)$_3$]In

Table 2.5 NMR results for [HB(3-phpz)$_3$]In

NMR	Peak Numbers, δ (ppm)
^{1}H	0.125, 1.75, 1.76, 1.77, 1.78, 1.80, 1.82, 2.02, 2.03, 2.04, 2.05, 2.06, 2.07, 2.08, 2.96, 3.59, 3.61, 2.64, 6.47, 6.68, 6.87, 7.17, 7.25, 7.28, 7.31, 7.70, 7.82, 7.85
^{13}C-Coupled	28.19, 28.47, 28.76, 29.06, 29.33, 29.62, 29.89, 205.65
^{13}C-Decoupled	25.34, 28.16, 28.45, 28.74, 29.02, 29.31, 29.60, 29.88, 100.69, 125.36, 126.12, 128.22, 128.59, 135.20, 136.03, 205.01, 205.57, 205.75

CHAPTER 3

SYNTHESIS OF INDIUM NANOPARTICLES

3.1 Introduction and Literature Review

Nanoparticles (derived from Greek word "*nanos*", meaning dwarf or extremely small) refer to small clusters of atoms about 1 to 100 nanometers long. The properties of nanoparticles of a material differ from that of its bulk. Nanoparticles have gained tremendous attention in the past few decades due to their high surface to volume ratio, special optical properties, wear resistance and chemical/heat resistance [61]. These particles are finding applications in various fields of technology including cosmetics [62], medicine [63], material science[64] and electronics [65].

Indium is a metal with low melting point adopting a tetragonal structure in solid-state. The tetragonal structure may or may not be preserved by size reductions [66]. While indium nanoparticles have been sparingly used so far, nanoparticles of indium oxides, and indium's oxides with other metals, have been reported to have applications in gas sensors [67], lubricants [68], photocatalysis [69], DNA hybridization [70] and semiconductor electronics [71]. Indium nanoparticles have been prepared using sodium reduction [72], solution dispersion [68], irradiation of bulk indium [73], laser ablation [74], metal vapor deposition [66] and decomposition of metallic-organic compound [75].

Khanna *et al.* have reported [72] a preparation of nanocrystalline indium particles by direct reaction of sodium metal with anhydrous indium trichloride in N,N-

37

dimethylformamide (DMF) or n-trioctylphosphine (TOP) as a solvent at 120 and 360 °C under argon atmosphere. In^{3+} ions were reduced to metallic indium(0) by Na in the solvent. The solvent acts as a dispersion medium for the nanoparticles and as a particle growth terminator. TOP seems to form an organic-cap on the nanoparticles thus controlling particle size. Indium nanoparticles prepared using this method have been found to have crystalline nature and a uniform particle-size distribution (15 nm for DMF and 50 nm for TOP). Nanoparticle size was found to be solvent dependent but not temperature dependent.

Zhao *et al.* have reported [68] a novel method of preparing indium nanoparticles from bulk indium involving surface oxidation and dispersion of indium droplets in an oil medium. Bulk indium in paraffin oil was stirred vigorously at 180 °C (above the m.p. of indium, 156.6 °C) in the presence of oxygen for 6 h. Then the solution was cooled, centrifuged and washed with chloroform to obtain nearly monodisperse (characterized by particles of uniform size in a dispersed phase) indium nanoparticles of size ranging from 15 to 30 nm. The outer layer was oxidized to indium oxide upon cooling. The layer of paraffin oil adhered to the outer oxide layer and acts as a surfactant to prevent agglomeration of nanoparticles.

Chaudret *et al.* have synthesized [75] indium nanoparticles by decomposition of organometallic precursor $[In(\eta^5-C_5H_5)]$ at room temperature in dry anisole containing polyvinylpyrolidone (PVP) (a polymer) or tri-n-octylphosphine (a ligand) oxide as stabilizer. This method produced indium nanoparticles with size in 2 – 8 nm range (normal distribution, mean = 5, σ = 3). It was deduced [75] that these nanoparticles have body-centered tetragonal phase of In^0, and they exhibited semiconducting properties.

The semiconducting indium nanoparticles are of special interest for applications [67] in microelectronic devices and gas sensors.

3.2 Materials

Sodium ($\geq$99%, pieces stored under heavy mineral oil), paraffin oil (analytical grade), N, N-dimethylacetamide (DMAc) (99% pure), methoxybenzene (anisole) (98% pure), toluene (99.8% pure), chloroform ($\geq$99%, with amylenes as stabilizer), and indium [powder, -100 mesh, 99.99% (metals basis)] were from Sigma-Aldrich and used as recieved. Indium (I) Chloride (InCl) (anhydrous, 99.995%) was from Alfa Aesar. [HB(3-phpz)$_3$]In was prepared by the procedure described in Section 2.2.4.4 and used. Sodium and InCl were stored and handled in nitrogen atmosphere dry box. DMAc and anisole were dried by refluxing with calcium hydride overnight under nitrogen. Toluene was dried by refluxing overnight under nitrogen with sodium and benzophenone to dry and monitor air and moisture. All solvents were distilled before use.

3.3 Preparative Methods

We have synthesized indium nanoparticles from three methods: 1) sodium reduction of indium(I) chloride; 2) dispersion of bulk indium in oil medium; 3) sodium reduction of indium complex ([HB(3-phpz)$_3$]In). Indium nanoparticles prepared using the three methods were re-dispersed in different solvents (toluene, chloroform and THF for method 1, 2 and 3 respectively) for preparing scanning electron microscopy (SEM) samples. The dispersions thus obtained were deposited on glass cover slip or oxide coated silicon substrate from their respective solvents by slow evaporation for

characterization. Samples were sputtered with 4 nm thick layer of gold and were visualized under Hitachi® SU-70 Ultra High Resolution Schottky FE-SEM.

3.3.1 Sodium Reduction of InCl

We have adopted synthetic route for indium nanoparticle preparation by reduction of $InCl_3$ described in the literature [72]. InCl is highly sensitive to air and moisture as opposed to relatively stable $InCl_3$. Hence, the preparation was carried out such that indium(I) was not exposed to atmosphere (moisture and air) until indium(I) reduced to indium(0). Freshly prepared InCl (1.5 g, 0.01 mol) and freshly cleaved sodium (0.23 g, 0.01 mol) were added to a Schlenk vessel in the dry box. Then the Schlenk vessel was connected to the vacuum line and was pumped down to 10^{-5} mm Hg. Dry, distilled DMAc was transferred to the vessel through vacuum distillation. It is crucial to avoid any moisture in handling the solution because it could produce hydrogen gas on contact with water and cause an explosion. The solution was stirred under vacuum at 120 °C for 4 h. The reaction solution was cooled and centrifuged (10 min at 6000X g) to obtain a light brown suspension. The suspension was stripped from its solvent under vacuum, washed with ethanol and water to remove unreacted sodium, and NaCl produced. The precipitate was then re-dispersed in toluene. The toluene suspension solution was centrifuged (10 min at 6000X g) again to remove any agglomerated particle. The experiment was repeated at 160 °C, keeping other parameters constant. Both solutions were separately diluted (5X, 10X, 20X and 40X) with toluene and used for characterization. 5 µL aliquot of each sample was pipetted on glass cover slip and solution was allowed to evaporate under fume hood and then dried by blowing nitrogen

gas over them. The dried samples were sputtered with 4 nm gold layer and then characterized using FE-SEM.

3.3.2 Solution Dispersion of Bulk Indium

Preparation method for indium nanoparticles by solution dispersion method has been adopted from reference [68]. Indium powder (5 g) was added to Paraffin oil (30 mL) in a 100 mL round bottom flask. The setup was maintained at 180 °C (using J-KEM® Digital Temperature Controller (Model 260/Timer)) and stirred vigorously for 10 h. The flask was bubbled with oxygen gas to allow oxidation of the outer layer of the particles being formed. The mineral oil solution was cooled and centrifuged (10 min at 6000 X g) to obtain a light gray suspension. The suspension was washed with chloroform several times and the washings were collected. The chloroform solution was transferred to a round bottom flask and then dried under vacuum distillation (10-12h) to form a fine gray powder deposited on the walls of the flask. The gray powder was then redispersed by adding chloroform (1 mL) into the flask by vacuum condensation to obtain a stock solution. The stock solution was diluted (5X, 10X, 20X and 40X) with chloroform and used for characterization. A 5 µL aliquot of each sample was pipetted on thermal oxide coated silicon substrate. The solution was allowed to evaporate under fume hood and then dried by blowing nitrogen gas. The SEM samples were sputtered with 4 nm gold layer and then characterized using FE-SEM.

3.3.3 Sodium reduction of {[HB(3-phpz)$_3$]In}

The coordination complex {[HB(3-phpz)$_3$]In} (1.130 g, 0.002 mol) and freshly cleaved sodium (0.05 g, 0.002 mol) were added to a Schlenk vessel in the dry box. The Schlenk vessel was hooked up to the vacuum line and pumped down to 10^{-5} mm Hg.

Dry, distilled DMAc was transferred to the Schlenk through distillation so that the compound is submerged in the solvent. The mixture was gently heated until the solvents were completely dissolved. The solution was stirred under vacuum at room temperature for 4 h. The product was then dispersed by distilling THF (5 mL) into the flask to obtain a cloudy suspension. The suspension was centrifuged for 10 min to obtain a clear filtrate. The filtrate was transferred to a round-bottom flask and then dried under vacuum (10-12 h). No heat was applied at this stage. Fine light-gray powder was deposited on the walls of the flask. The product was redispersed by distilling THF (1 mL) into the flask to obtain a stock solution. The stock solution was diluted (5X, 10X, and 20X) in THF and used for characterization. A 8 μL aliquot of each sample was pipetted on glass cover slip. Solution was allowed to evaporate under fume hood and then dried by blowing nitrogen gas. SEM samples were sputtered with 4 nm gold layer and then characterized using FE-SEM.

3.4 Observations and Results

3.4.1 Sodium Reduction of InCl

The solvent, DMAc has been reported [76] as a good dispersion medium for nanoparticles synthesis, to act as a particle growth terminator and to prevent aggregation of nanoparticles [77]. The reaction between InCl and sodium began as soon as the solvent was transferred into the Schlenk vessel. Sodium particles dissolved completely within 1 h. The colorless solvent turned to dark gray as the solutes were dissolving. Then the color changed to dark brown as temperature was raised. Equation for reduction of indium(I) to indium(0) is as follows:

$$InCl + Na \rightarrow In^{(0)} + NaCl$$
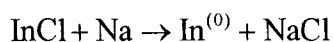
The final product was obtained as a suspension in toluene. The sample was allowed to dry at room temperature for 1 h and was dried. The suspension had to be diluted and centrifuged several times to get more uniformly distributed particles. Analysis of sample prepared from 20X stock solution by SEM indicate good spatial dispersion of particles. SEM micrograph of the sample (20X stock solution) is shown in Figure 3.1. Particle size was estimated by measuring diameter of 10 particles using image processing tools. It was estimated that diameters of the particles obtained were in 90 – 100 nm range. The size estimation of the particle is approximate due the charging effect (nonlinearity in lateral dimensions due to charge accumulation on sample), inherent to SEM.

The composition of the particles was analyzed using energy dispersive X-ray (EDX). Silicon, aluminum, potassium and partly sodium peaks seen in the graph (Figure 3.2) are from the glass substrate. Composition of indium in the particles was determined to be ~52% by weight (after baseline correction for the glass substrate was applied).
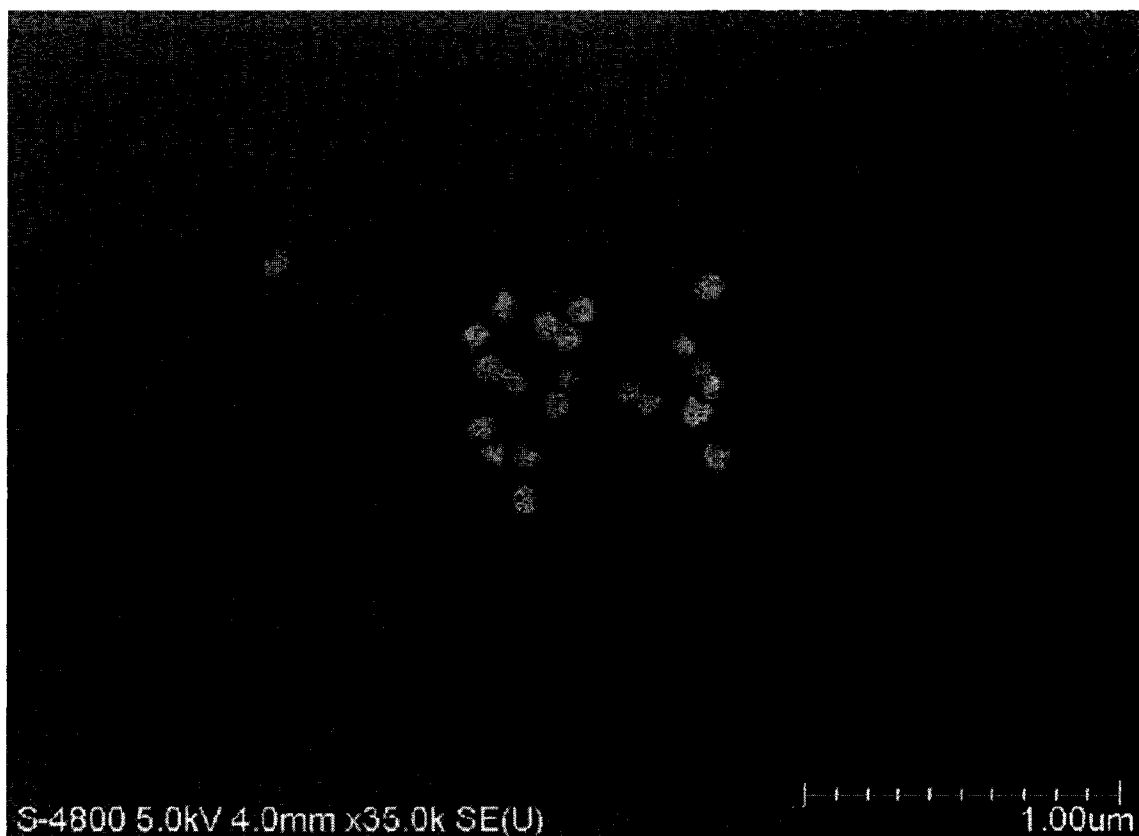
Figure 3.1 SEM micrograph of indium nanoparticles from sodium reduction of InCl
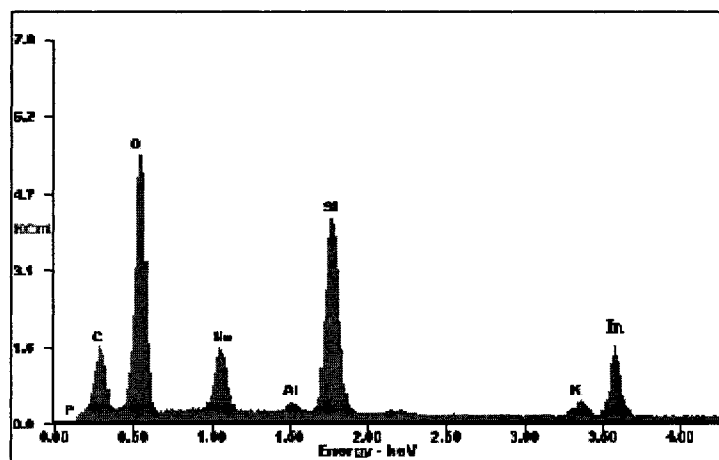
Figure 3.2 EDX Data for indium nanoparticles from sodium reduction of InCl. Emission energy is plotted against K_α count

3.4.2 Solution dispersion of bulk indium

A gray colloidal solution was formed as described in Section 3.3.2, as the temperature reached 160 °C (melting point of indium = 156 °C). The product turned darker after cooling. The solution was centrifuged to obtain a light gray suspension. The paraffin oil suspension was washed with chloroform and centrifuged again. SEM micrograph of 10X stock solution showed spherical particles with diameters in the 100 nm – 1 μm range (Figure 3.3). Irregularly shaped fragments were also seen in the micrograph. EDX for the same sample showed ~85 % indium by weight (after baseline correction for SiO_2 substrate was applied) (Figure 3.4). High percentage of indium in the sample indicates that the both the spherical particles and the fragments contain indium. Surface oxidation of indium and adsorption of the paraffin oil produces additional peak for oxygen and carbon.
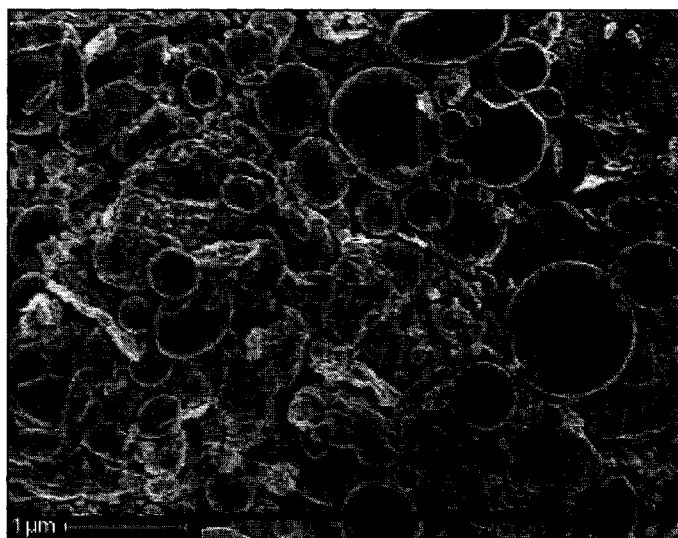
Figure 3.3 SEM micrograph of indium nanoparticles from solution dispersion of bulk indium
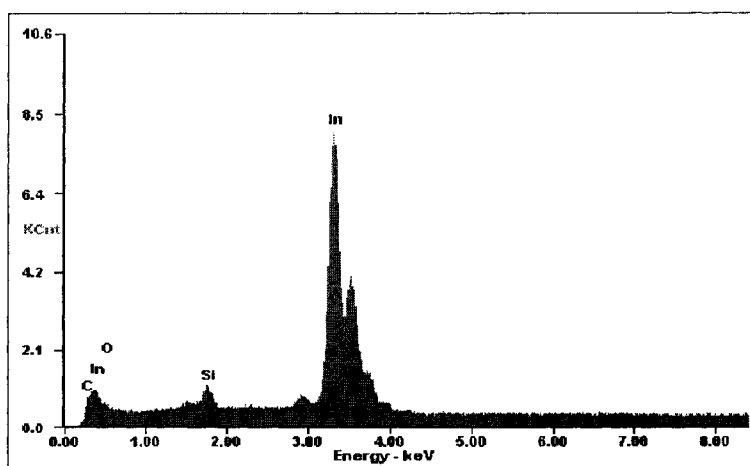
Figure 3.4 EDX spectrum for indium nanoparticles from solution dispersion of bulk indium. Emission energy is plotted against K_α count.

3.4.3 Sodium Reduction of [HB(3-phpz)₃]In

A light gray cloudy suspension formed as DMAc was transferred to the solid reactants as described in Section 3.3.3. The solution turned darker as the reaction progressed. The solvent was stripped from the product using vacuum. Gentle heating was required during this process. The yield of product was less than 0.05 g (22 % yield). SEM analysised of the product showed uniformly dispersed particles with diameters in 10-50 nm range for 20X stock solution (Figure 3.5). However, the particle shape was irregular. EDX analysis of the sample revealed that the nanoparticles are composed of ~27 % indium by weight (Figure 3.6) (after baseline correction for the glass substrate was applied).

**Figure 3.5** SEM micrograph for indium nanoparticles from reduction of {[HB(3-phpz)₃]In}
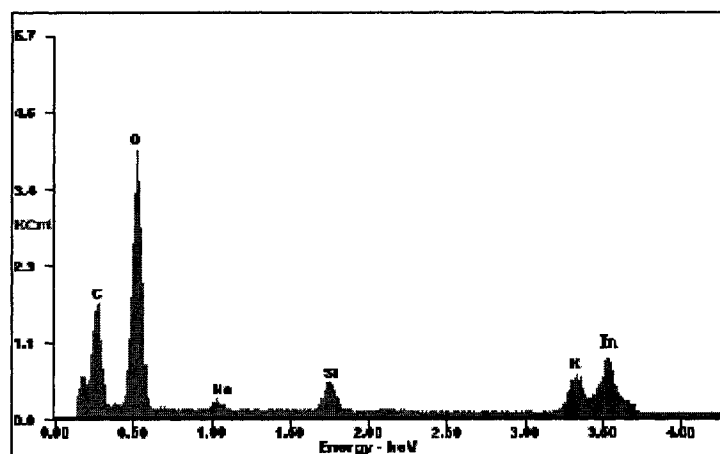
Figure 3.6 EDX spectrum for indium nanoparticles from reduction of [HB(3-phpz)₃]In. Emission energy is plotted against K_α count

Information on size distribuition, shape, and dispersion of indium nanoparticles prepared by the above three methods has been used to select the appropriate method for subsequent deposition of the indium nanoparticles on DNA template. Monodispersed indium nanoparticles formation from reduction of {[HB(3-phpz)$_3$]In} indicates that it is possible to reduce {[HB(3-phpz)$_3$]In} on DNA molecules *in-situ*, resulting in non-aggregated deposition of indium(0) on DNA strands.

Comparison of particle size, shape and nature of dispersion of the nanoparticles prepared by three methods described above is tabulated in Table 3.1. Indium nanoparticles prepared using solution dispersion has relatively large particles and is partially aggregated. The large size and agglomeration makes this method unsuitable for deposition on a DNA template to construct nanowires. However, indium nanoparticles prepared from sodium reduction of InCl and {[HB(3-phpz)$_3$]In}have relatively smaller size and are dispersed uniformly on the substrate. These properties open up the possibility of obtaining uniform metal deposition on DNA template by either depositing indium nanoparticles from sodium reduction directly on to immobilized DNA template or by reducing [HB(3-phpz)$_3$]In on DNA molecules *in-situ*. Metallization of the DNA template on a substrate forming DNA nanowires is discussed in the following chapter.

Table 3.1. Comparison of properties of nanoparticles

Method	Particle Size (nm)	Shape	Spatial Dispersion
Sodium reduction of InCl	90-100	Roughly spherical	Uniform
Solution dispersion of bulk indium in mineral oil	100-1000	Mixture of spherical and irregular	Partial aggregation
Reduction of {[HB(3-phpz)₃]In}	10-50	Irregular	Uniform

CHAPTER 4

DNA-INDIUM INTERACTION STUDIES

4.1 Introduction

It was widely [20] recognized that deoxyribonucleic acid (DNA) has the appropriate molecular-recognition and mechanical properties suitable for a nano-sized device on electronic circuits. Intrinsic electrical conductivity of DNA molecules has been gaining attention and has been an issue of debate for the past decade. It has been recently reported [78] that intrinsic DC conductivity of immobilized lambda phage double-stranded DNA molecule is 4×10^{-15} AV^{-1} μm^{-1} under low humidity argon atmosphere. Such a low conductivity renders unmodified DNA molecule unusable as electrical interconnects. Moreover, the conditions in nano-circuits will be drastically different from DNA's natural biological environment, causing DNA molecules to denature and disintegrate in the absence of buffer solution and counterions. It was suggested [20] that electrical functionality can be instilled into DNA molecules by depositing metal along the length of a stretched DNA molecule. Braun *et al.* demonstrated [20] successful chemical deposition of silver on DNA using complex formation reactions between silver and DNA bases.

At equilibrium, a DNA molecule in aqueous solution will usually be randomly structured as a result of thermal motion. Entropy factors tends to shorten the end-to-end distance to a much smaller size than the contour length, depending on the environment.

50

A DNA molecule therefore must be stretched between two electrodes to serve as a nanowire template. Many approaches have been used to stretch and align DNA molecules: molecular combing [79], electrophoretic stretching [80], hydrodynamic stretching [81], and Van der Waals interaction [82]. A common strategy is to tether one end to a surface and then to stretch the molecule by an external force, for example surface tension.

DNA-templated assembly of nanowires has been an integral part of progress in nanowire fabrication in the past few years. A variety of metallic nanowires have been made using DNA templated approach: palladium [21-23], platinum [24, 26, 83], gold [60-64], copper [84-86], and cobalt [87]and nickel [88].

The most commonly used approach for DNA metallization is an electroless plating procedure involving reduction of metal ions already bound to DNA electrostatically. This method relies on the electrostatic and chelating interactions between DNA and ionic metal species. For example, Braun *et al.* [20] reduced DNA-bound silver ions using hydroquinone to produce silver nanoparticles. Ag(I) ions bind to DNA by Ag-Na ion exchange. Hydroquinone reduces DNA-bound Ag(I) ions to Ag(0) metallic clusters, which then autocatalyze further reduction of Ag ions in the solution. DNA stretching and positioning was achieved by Au thiol coupling and hydrodynamic flow. Figure 4.1 shows a prepared Ag nanowire between two Au electrodes. The diameter is ~100 nm (Figure 4.1A). The resistively, 3.4×10^{-3} (Figure 4.1B), is higher than that of bulk silver. Nevertheless, this method has become the prototype for metallization of single DNA molecules. Another recently demonstrated [86] method of DNA-templated nanowire fabrication uses nonspecific metallic deposition. Alkali metal

cations with high affinity for SiO_2 were used to passivate the silicon surface, creating a physical and an electrostatic barrier against nonspecific silver or copper cation adsorption and subsequent metal deposition. For silver nanowires synthesized from single-stranded DNA, this ionic masking strategy leads to a 51% reduction in the number of nonspecifically deposited nanoparticles and an even greater decrease in their dimensions [86].
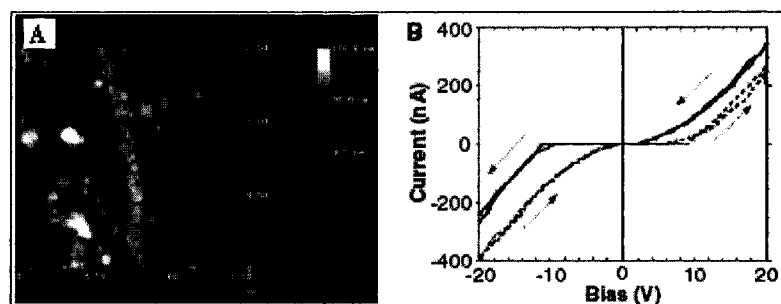
Figure 4.1 Characterization of metallized DNA. A) Atomic force microscope (AFM) micrograph of 100 nm wide Ag nanowire using DNA-templated assembly. B) I-V characteristics of the nanowire. Reprinted from reference [20]. Copyright 1998 Macmillan Publishers Ltd.

The binding of metal cations to the DNA molecule can play an important role in determining its conductivity. A type of DNA-metal ion complex known as M-DNA, with divalent metal ions (Zn^{2+}, Ni^{2+} or Co^{2+}) bound, has been described [89]. M-DNA consists of GC and AT base pairs in which the imino proton of guanine and thymine have been replaced by a Zn^{2+} ion to form a wire of zinc ions sheathed by DNA helix [90]. DNA-metal ion interaction studies have so far been mainly conducted to determine effects of metals on biological properties such as toxicity [91], carcinogenicity [92] and antitumour activity [93].

We have investigated the interaction of indium(III) ions with DNA molecules in aqueous solution using spectroscopic, fluorescence and gel electrophoresis techniques. DNA-indium(0) and DNA-indium(I) interaction were investigated using SEM characterization of samples prepared by indium species in aprotic polar solvent (toluene and THF) deposited on DNA immobilized on a glass substrate. In this chapter, a discussion of affinity of indium species to DNA molecules is presented to give the extent of DNA metallization and its structure during nanowire formation.

4.2 Indium(III)-DNA Interaction Studies

4.2.1 Materials

The λ DNA (10 mM Tris, 1 mM EDTA stock solution 45% G-C) from *E. coli* host strain W3110, and sodium salt of CT DNA (highly polymerized, type I, 42 % G-C) were purchased from Sigma-Aldrich (USA) and used without further purification. The ratio of absorbance at 260 nm and at 280 nm (A_{260}/A_{280}) for λ-DNA and CT DNA were 1.77 and 1.88, respectively, indicating that the preparations were mostly free of protein [94]. The DNA concentration per nucleotide (or phosphate) was determined by observing the absorption ($\epsilon_{258} = 6600$ M^{-1} cm^{-1}) [94]. Crystalline indium(III) chloride (98% pure), EDTA (anhydrous, 99%) and EtBr were also purchased from Sigma-Aldrich and used as received. All solutions were prepared using 18 MΩ-cm water from a Milli-Q purifier (Millipore, USA). CT DNA stock solution was prepared by dissolving the DNA in 10 mM Tris pH 7.5 to a final concentration of 1 mg/mL and gently mixing overnight. DNA samples were stored at 4 °C for not more than a week for use in experiments. Freshly prepared InCl$_3$ solutions were used within 4 h and 25 mM EDTA solution was

prepared by dissolving solid EDTA in water. All experiments besides thermal denaturation of DNA were carried out at 22-24 °C.

4.2.2 Experimental Techniques

4.2.2.1 UV spectroscopy

All UV spectra were obtained with a Shimadzu 1650PC UV-vis spectrophotometer (Japan). Samples were analyzed in a quartz cuvette with a 1 cm path length. An attached Fisher Scientific Isotemp 3006 water bath with a circulator pump (USA) was used for DNA melting experiments. Stock solutions of CT DNA and λ DNA were diluted with 5 mM Tris solution at pH 7.5 to a final DNA concentration of 50 μg/mL. The 10 μL aliquots of 5 mM or 10 mM $InCl_3$ were titrated against 2 mL DNA solution in a cuvette. The solution was stirred by repeated gentle in/out pipetting with a 1000 μL micropipette for 30 s and then allowed to sit for 1 min before recording the spectrum for each indium ion concentration. The micropipette tips were large enough to minimize shearing of DNA molecules. Incubation times of 1 min, 10 min, and 1 h were tested. The spectral variations after 1 min were negligible, suggesting that binding equilibrium was reached on this time scale. Subsequenty, kinetic spectroscopic studies at 260 nm also revealed that spectral changes were insignificant after 30 seconds to 1 minute of mixing $InCl_3$ solution with DNA solution. Absorption study during the titration of 25 mM EDTA against DNA solution was carried out to test the chelating effect of EDTA on indium ions. Absorbance readings were adjusted to account for the dilution of DNA by the titrant.

4.2.2.2 <u>CD Spectroscopy</u>

Circular dichroism (CD) spectra of CT DNA solution in the presence and absence of $InCl_3$ were measured with a Jasco J-810 circular dichroism spectropolarimeter (Japan) in a 1 mm-path length quartz cuvette. The wavelength range was 200 nm-300 nm with the instrument settings: step size, 0.1 nm; scanning speed, 0.3 nm s^{-1}; response time, 0.3 s; number of scans, 50. The results are presented as differential absorption in milliabsorbance units.

4.2.2.3 <u>Extrinsic Fluorescence Emission</u>

Fluorescence quenching and recovery experiments were done with a TECAN GENois microplate reader (USA). Same concentrations of $InCl_3$ and CT DNA as in titration experiments were used, and the concentration of EtBr was 0.1 $\mu g/mL$ (ϵ_{478} = 5680 M^{-1} cm^{-1} [95]). A 96-well microplate was used for the experiment. Twelve samples were prepared by varying the concentration of $InCl_3$ in DNA solution such that the molar concentration ratio, $[In^{3+}]/[DNA$ base pairs] (R), varied from 0 to 3.5. The molar concentration of DNA base pairs was calculated assuming that the average base pair molecular weight is 660 Da. A 100 μL quantity of each sample was added to separate wells in the microplate. A 12-well concentration gradient of EDTA was obtained by maintaining R = 3.5 while changing the concentration of EDTA from 0 to 2.5 mM. Three identical samples were prepared independently for each $InCl_3$ concentration to ensure repeatability. Samples were excited at 360 nm. Fluorescence emission was measured at 610 nm. Fluorescence emission F_i for each well was calculated as the average of the three samples. The emission data are presented as F_i/F_0, F_0 being the F_i value for DNA-EtBr complex in the absence of indium(III).

4.2.2.4 <u>Gel Electrophoresis</u>

20 μL 50 μg/mL CT DNA, 0.1 μg/mL EtBr with R = 0-2 was introduced into a

well in a 0.75 % (w/v) agarose gel (40 mM Tris, 50 mM boric acid, 1 mM EDTA, pH

8.0) and incubated for 1 h at 25 °C. The DNA samples migrated in the gel on application

of an electric field of 5 V/cm for 4 h. DNA mobility was assessed qualitatively by

visualization with a Spectroline UV transilluminator (USA) equipped with a light shroud

and an Olympus digital camera (Japan).

4.2.3 Results and Discussions

4.2.3.1 <u>Spectrophotometric Titration</u>

Both λ DNA and CT DNA showed moderate hyperchromicity (increase in

absorbance) followed by significant hypochromicity (decrease in absorbance) on

increasing the concentration of InCl$_3$. These changes were accompanied by a

bathochromic (shift of absorbance towards longer wavelength) shift of ~4 nm near 260

nm. Absorbance and the corresponding peak shift for λ DNA and CT DNA are plotted

against R in Figure 4.2. R ranged from 0-2 (CT DNA experiments, 0-0.26 mM InCl$_3$) or

0-2.5 (λ DNA, 0-0.37 mM InCl$_3$). Absorbance near 260 nm increases steadily with R

(up to 30 % for CT DNA and 20 % for λ DNA) before dropping (up to 20 % CT DNA

and 30 % for λ DNA) and remaining steady thereafter (Figure 4.2A, C).
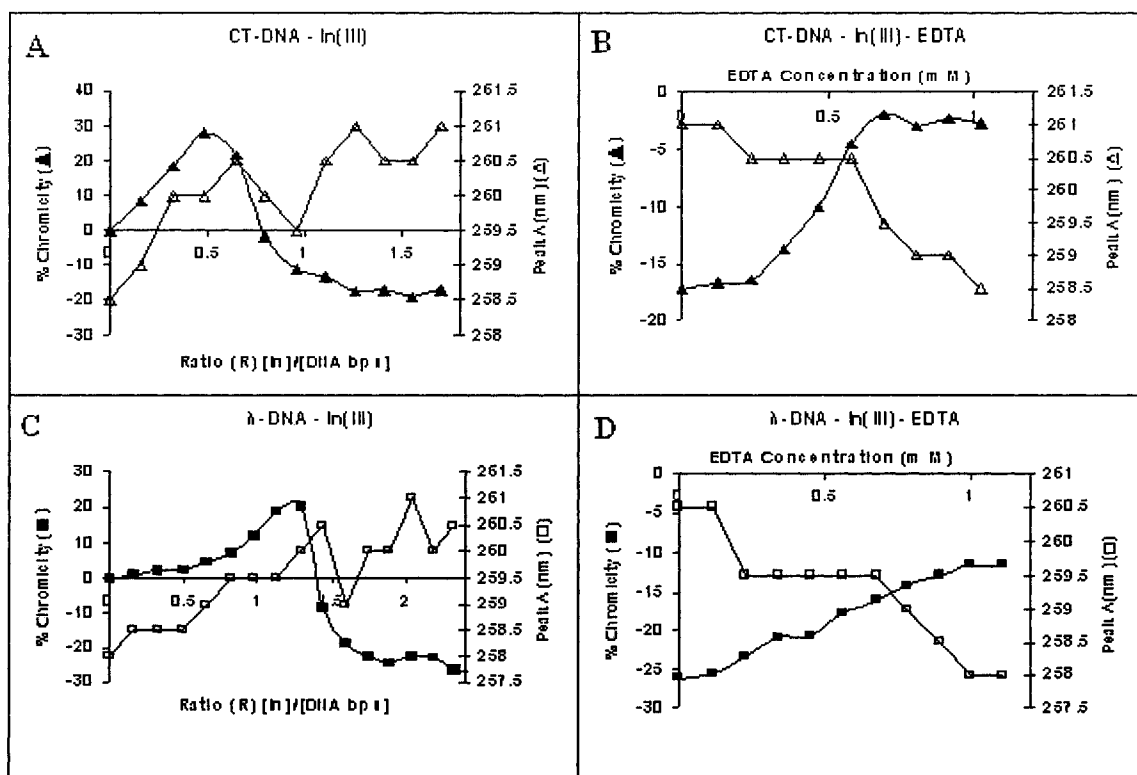
Figure 4.2 DNA-Indium titration curves. A) CT DNA v/s R. B) λ DNA v/s R. Primary X-axis: R, primary Y-Axis: absorbance max change, represented in terms of percentage (% Chromicity), secondary Y-Axis: wavelength at maximum absorbance (Peak). C) R = 2, [CT DNA] = 50 μg/mL v/s [EDTA]. D) R = 2.5, [λ DNA] = 50 μg/mL v/s [EDTA]. Primary X-axis: EDTA concentration (mM), primary Y-Axis: absorbance max change, represented in terms of percentage (% Chromicity), secondary Y-Axis: wavelength at maximum absorbance (Peak).

CT DNA was also titrated against NaCl in the range 0-5 mM as a control for the possibility that Cl⁻ ions influence absorbance (data not shown). The concentration of NaCl in DNA samples was chosen to mirror the $InCl_3$ experiments (ionic strength of $InCl_3$ is 6x that of NaCl in dilute solution). NaCl did not influence absorbance at any concentration in the indicated range. Control experiments were also done at a lower DNA concentration (0.25 μg/mL), maintaining R and other conditions. The behavior of DNA was similar under both conditions.

R', defined as the R value at the mid-point of the hypochromic slope, represents the mid-point of the structural transition. It can be seen in Figure 4.2 that spectroscopic titration curve for both λ DNA and CT DNA behave in a similar manner. The slight difference in R' values suggests that EDTA in the stock solution of λ DNA might chelate indium ions and therefore yield a higher apparent value of R' for λ DNA. The difference in hyperchromic (increase in absorbance) and hypochromic (decrease in absorbance) effects between CT DNA and λ DNA can be ascribed to the difference in counterions and buffer concentration in the respective stock solutions, as well as the difference in G-C content (42 % for CT DNA [96] and 45 % for λ DNA [97]).

The hypochromic effect due to interaction of DNA with indium ions was found to be largely reversible by addition of the metal ion chelator, EDTA (up to 80 % of the initial value for CT DNA, up to 60 % of the initial value for λ DNA). Figure 4.2B, D show the effect of increasing EDTA concentration on absorbance of the CT DNA-In^{3+} solution (R = 2) and the λ DNA- In^{3+} solution (R = 2.5), respectively. These experiments suggest a 15-20 % recovery of absorbance for both species of DNA in the presence of EDTA. A hypsochromic shift of ~4 nm also occurred on addition of EDTA.

Figure 4.3 presents a family of UV spectra for λ DNA at different concentrations of InCl$_3$ and EDTA. The inset shows data in the range 240-280 nm. Absorbance changes in the far UV region, though significant, were not analyzed more thoroughly because many other chemical species, e.g., Tris, EDTA, and Cl$^-$, absorb in this region. The spectral properties of CT DNA under the same conditions were found to be similar to those of λ DNA.
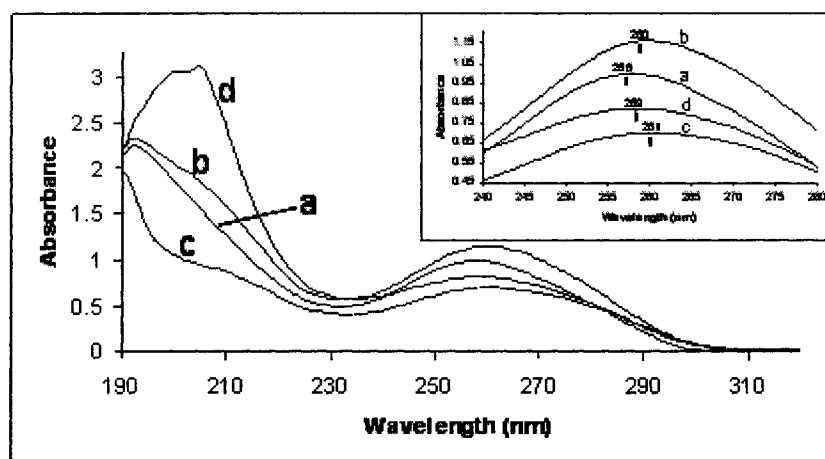
Figure 4.3 UV-Vis spectrum (320 – 190 nm) for λ DNA. (a) r=0, (b) R = 1.2, (c) R = 2.5, (d) R = 2.5 and [EDTA] = 0-1.5 mM. Inset: Expanded view of spectrum in 240 – 280 nm range.

The effect of counterions on In^{3+}-DNA binding was tested by varying the NaCl in the range 0-40 mM but keeping all other conditions same. Na^+ ions were found to affect the value of R' and the maximum hyperchromism and maximum hypochromism (Figure 4.4). The data suggest that the effect of counterions is particularly significant in the 0-10 mM range.
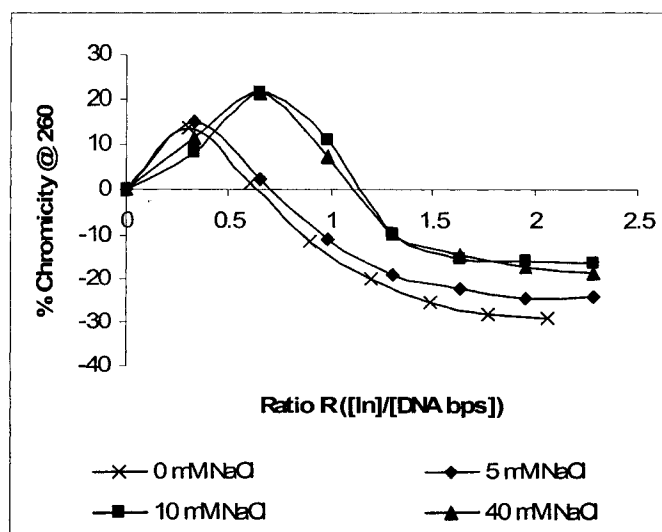
Figure 4.4 Titration curve for CD DNA in presence of Na^+ ions. Change in absorbance for CT DNA at 260 nm represented in terms of % chromicity, plotted against ratio R in presence of NaCl concentrations 0, 5, 10 and 40 nM

4.2.3.2 Melting Experiments

Thermal denaturation curves were obtained for CT DNA with R = 0, 0.8 and 2. As evident in Figure 4.5, T_m increases with increases in R, from 45 °C for R = 0 to 57 °C for R = 4. The increase in T_m is accompanied by a broadening of the transition and a reduction in final hyperchromicity (20 % for R = 0, 15 % for R = 1.5, and 5 % for R = 4). The results indicate that the interaction of CT DNA with In^{3+} ions stabilizes the DNA double helix. That is, In^{3+} binds with greater affinity to the double-stranded molecule than to single strands. The spectra data would also suggest, however, that the binding process distorts the conformation of DNA.
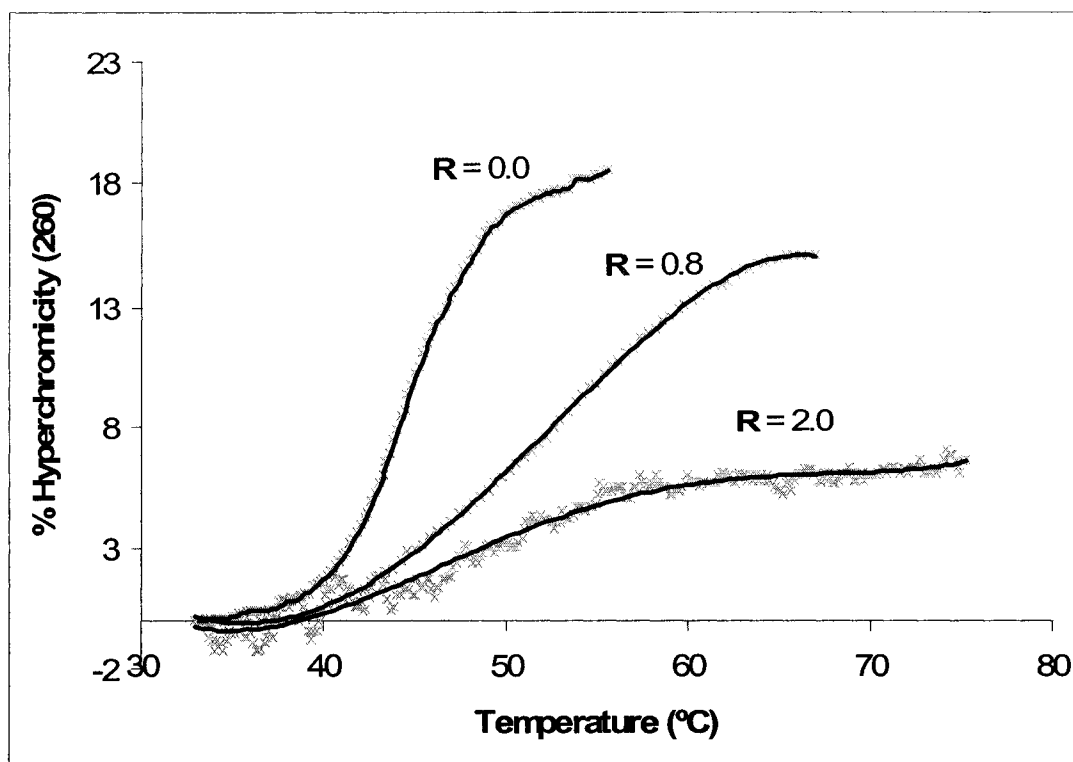
Figure 4.5 Melting Curves for CT DNA. Thermal denaturation curve for CT DNA at R = 0.0, 0.8 and 2.0. Change in absorbance at 260 nm represented in terms of %Hyperchromicity plotted against temperature (°C)

4.2.3.3 CD Experiments

Structural changes in DNA on addition of $InCl_3$ were studied by CD at different values of R (R = 0, 0.15, 0.3, 0.5, 1, 1.5) (Figure 4.6). Figure 4.6 shows the differential absorbance for characteristic Cotton effects at 217, 245 and 275 nm at various R values. In all cases, peak intensity decreases as R increases from 0 to 1.5. Moreover, changes in the peaks decrease in magnitude as R increases from 0 to 1; there is negligible change above R = 1, suggesting saturation. Below 210 nm, the differential absorbance increased considerably at high values of R.
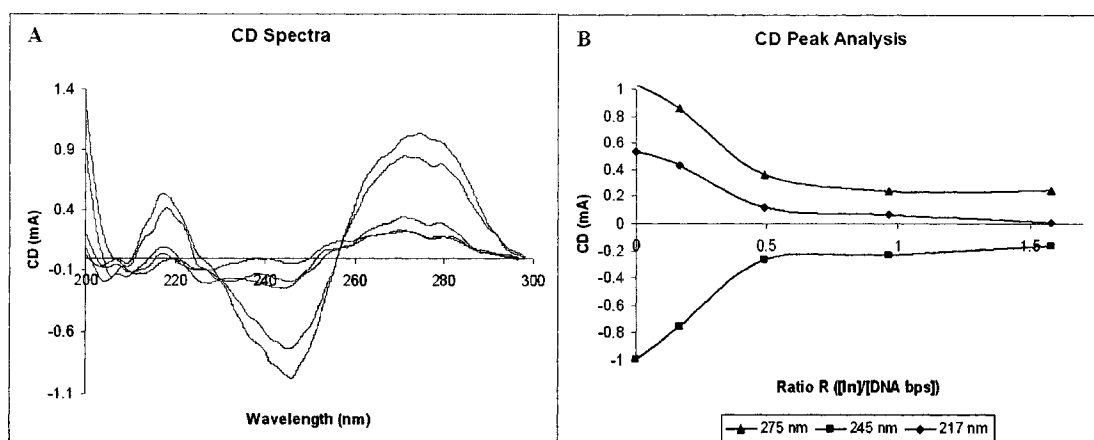
Figure 4.6 Circular Dichroism. A) CD spectra for CT DNA at various concentrations of InCl₃ (R = 0 – 1.6), are plotted as milliabsorption units versus wavelength. The spectrum is the average of 50 scans. B) Δε values for peaks (275 nm, 245 nm, 217 nm) for various concentrations of InCl₃ (R = 0 – 1.6).

4.2.3.4 Fluorescence Experiments

Relative fluorescence (F/F₀) of 50 μg/mL CT DNA and 0.1 μg/mL EtBr was measured as a function of R. Fluorescence emission of EtBr-DNA was quenched by In³⁺ ions, reducing the fluorescence intensity by around 25 % at R = 3.5 (Figure 4.7). The quenching profile is closely related to the hypochromicity profile (Figure 4.2); the transition in fluorescence intensity, however, occurs at a lower R value (R' = 0.25). The fluorescence recovery profile was obtained by adding EDTA to DNA-EtBr solution at R = 3.5, keeping all other conditions constant. The data show that EDTA could recover the fluorescence to about 60 % of its initial value. A control experiment with NaCl (analogous to the Na⁺ control in UVS experiments) showed that increases in Na⁺ ion concentration did not quench the fluorescence emission (data not shown).
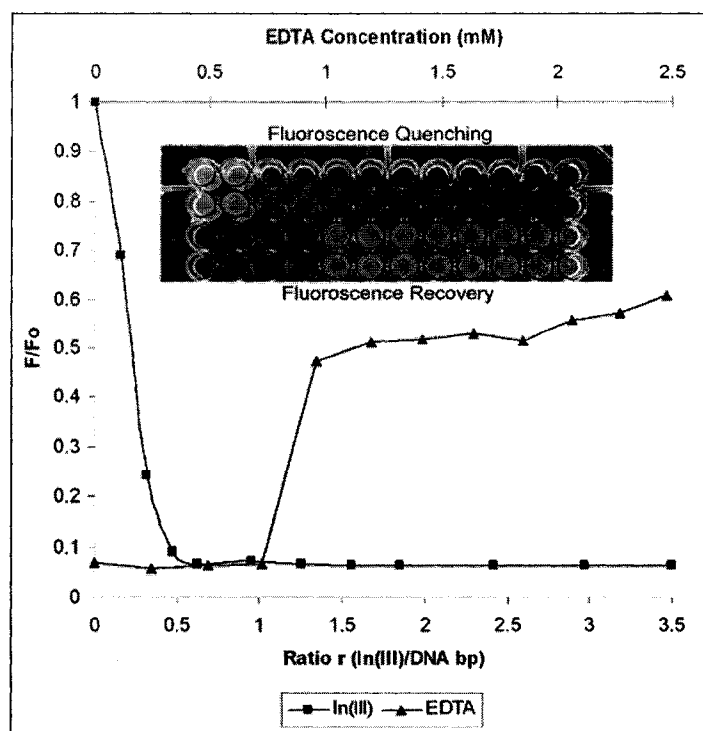
Figure 4.7 Ethidium Bromide fluorescence quenching and recovery profiles. F/F$_0$ as a function of R (square) and as a function of EDTA concentration (mM) with r = 3.5 (triangle). Square: Quenching Profile, [DNA] = 50 μg/mL, [EtBr] = 0.1 μg/mL, r = 0 – 3.5. Triangle: Recovery profile, [DNA] = 50 μg/mL, [EtBr] = 0.1 μg/mL, r = 3.5, [EDTA] = 0 - 2.5 mM. Inset: Image of 96 well microplate, row A & B; quenching, rows C & D; recovery.

.

4.2.3.5 Gel Electrophoresis

Lanes 1-7 in Figure 4.8 represent CT DNA solution with R = 0, 0.2, 0.4, 0.8, 1.5, 2.0, and 0, respectively. The concentrations of the various chemical species were same as in the fluorescence studies. EtBr-stained DNA is relatively fluorescent at R = 0 but steadily decreases as R increases to 2, where the fluorescence intensity is low. This decrease in band brightness is an obvious result of fluorescence quenching due to In^{3+}-DNA interaction. It is evident from the figure that there is no significant difference in mobility between the samples, despite the differences in InCl$_3$ concentration and fluorescence, and no apparent shearing of the DNA.

Figure 4.8 Gel Electrophoresis Image. Lane 1 – 7, R = 0, 0.2, 0.4, 0.8, 1.5, 2.0 and 0 respectively. (0. 50 μg/mL CT-DNA, 5 mM Tris (pH 7.5), 0.1 μg/mL EtBr).

A molecular model of 20 base-pair of mixed-sequence, right-handed B-DNA surrounded by 20 In^{3+} ions (R = 1) is shown in Figure 4.9. The van der Waals radius of In^{3+} is 0.93 Å [98]. The model gives an idea of the relative size of the interacting species.

Figure 4.9 Molecular Modeling of B-DNA. Modeled structure of mixed sequence dsDNA shown surrounded by In^{3+} ions at R = 1. Van der waal radius of indium in 3+ oxidation state is 0.93 Å.

The UV titration results presented here suggest that the DNA-indium interaction occurs in at least in two stages: low metal ion concentration (R < 0.5), where absorption increases, and high metal ion concentration (R > 0.5), where absorption decreases. There was no evidence of DNA aggregation up to R = 20. The initial hyperchromicity can be attributed to the electrostatic interaction between In^{3+} and the phosphate groups in DNA backbone [99]. A parallel analysis of UVS data and CD data indicates that the DNA undergoes a structural transition on interacting with In^{3+} and is then transformed into another conformation [100], [101]. The CD spectra for R = 1 and R = 1.6 closely resemble that of left handed Z-DNA [102]. This data suggests the possibility that the usual right-handed B-form shifts to the left-handed Z-form as the In^{3+} concentration increases. The decrease in the absorbance peak at 275 nm and 245 nm, together with the hypsochromic shift of the peak at 275 nm and the bathochromic shift of the 245 nm peak, is consistent with a conformation change from the B-form to Z-form [103]. A large decrease in the absorbance confirms a considerable coiling and condensation of the DNA molecules.

The UV absorption titration experiment revealed a hypochromic shift (20 %) and bathochromic shift (4 nm) of the absorbance peak at 260 nm upon saturation of indium binding sites. These data suggest that the binding of indium ions to DNA is more likely to occur by intercalaction than simple outside bonding [104, 105] . The interpretation is supported by the fluorescence quenching profile, where the binding of indium ions inhibits the intercalaction of EtBr molecules and leads to increased quenching with increases in R [89, 90]. The 190 nm–210 nm range of the absorption spectrum (Figure 4.2) shows obvious changes with changes in $InCl_3$ concentration.

EDTA is widely known to chelate most divalent and some trivalent metal ions by forming coordination compounds. A proposed structure of the indium-EDTA complex is shown in Figure 4.10 [106]. The observed recovery in absorbance and fluorescence on addition of EDTA might therefore be attributable to the formation of EDTA-In complexes, reducing the concentration of free In^{3+} ions and allowing the DNA molecules to return to their original confirmation in the absence of In^{3+}.
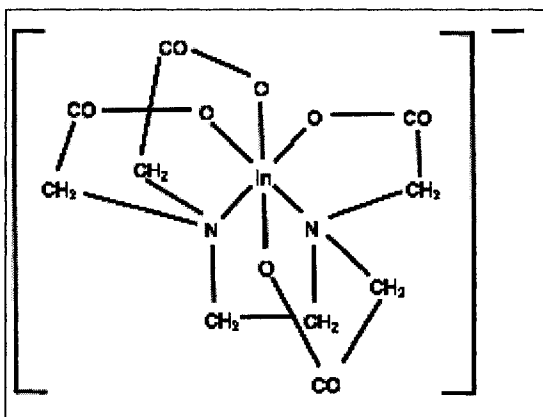
Figure 4.10. EDTA–In complex, EDTA can chelate indium in aqueous solution. Redrawn after reference [106]

4.3 [HB(3-phpz)₃]In-DNA Interaction Studies

4.3.1 Materials

Sodium salt of *calf thymus* (CT) DNA (highly polymerized, type I, 42 % G-C) were purchased from Sigma-Aldrich (USA). The stock solution of DNA was purified using QIAGEN®, QIAEX II Gel Extraction Kit. The concentration of the purified DNA was determined to be ~150 μg/mL (assuming coefficient of extinction at 258 nm (ϵ_{258}) = 6600 M^{-1} cm^{-1} [94]) and the ratio of absorbance at 260 nm and at 280 nm (A_{260}/A_{280}) was 1.88, indicating that the preparations were mostly free of protein [94]. 10X dilute

solution of indium nanoparticles from the reduction of [HB(3-phpz)$_3$]In (Section 2.2.3.3.2) in THF was used.

4.3.2 Methods

CT DNA was deposited on glass substrate by evaporation. Evaporation is a simple way to characterize molecular macroscopic conformations as a reference to stretched and combed DNA molecules. Stock solution was diluted in 10 mM Tris (HCl) buffer solution (pH 7.5) to obtain DNA concentrations of 100 ng/mL, 200 ng/mL and 500 ng/mL. 8 μL of diluted DNA solutions were pipetted on the glass substrates. DNA control samples were prepared by evaporating the excess solvent in the fume hood for 10-20 min, rinsing with water and drying by passing nitrogen gas.

THF solution of [HB(3-phpz)$_3$]In (0.1 M, 0.0565 g [HB(3-phpz)$_3$]In, 1 mL THF) was prepared in a 1.5 mL microtube. THF solution (10 μL) was pipetted on the DNA-coated glass substrate. The solution was allowed to dry under a fume hood for 10-12 min and then dried by passing nitrogen gas over it. Sodium (0.023 g) was added to Schlenk in dry box. Dry degassed DMAc (10 mL) was transferred to the a Schlenk vessel to dissolve sodium. The substrate and the sodium solution were taken into the dry box. DMAc solution of sodium (10 μL) was pippeted on the substrate. Untreated metallized DNA samples were prepared by drying excess solvent in the dry box (~2 h) and passing nitrogen gas. The samples were heat treated by gradually heating them to 157 °C in a Precision Scientific Thelco 19 Vacuum Furnace (Precision® Scientific Corporation, USA) equipped with a Welch® DuoSeal® vacuum pump working at 10^{-5} mm Hg. Furnace temperature was maintained at this temperature for 30 min and was allowed to cool to room temperature gradually. DNA control samples, untreated metallized DNA

samples and the heat treated metallized DNA samples were sputtered with 4 nm gold layer and imaged under SEM.

Preliminary investigations for electrical resistivity of glass substrate control, DNA control, untreated metallized DNA and heat treated metallized DNA samples were conducted using 2-point probe method on a Keithley probe station (Keithley[®] Instruments, USA). The setup for resistivity measurement is shown in Figure 4.11. The two probes were 1000 μm apart on the surface of the sample. Electrical resistance was measured at 3 different locations for each sample. Resistivity was determined using the following formula:

$$\rho = \frac{R \times A}{L}$$

Where, A (crossectional area) = 100 μm^2, assuming 2-D structure with tip contact diameter = 100 μm, R = Measured resistance and L (distance between the two probes) = 1000 μm.
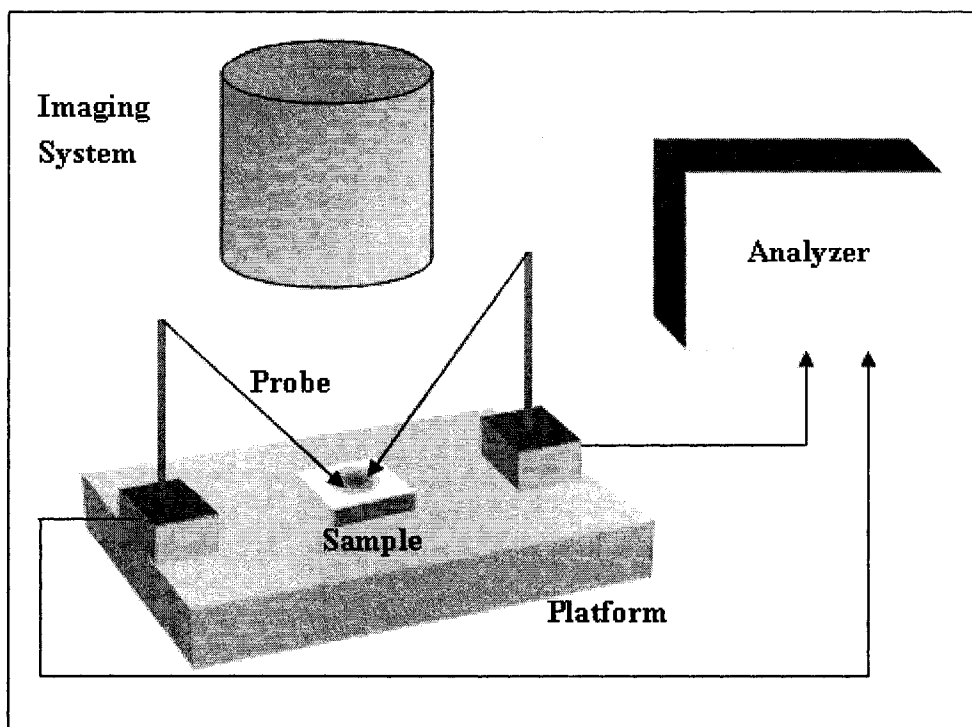
Figure 4.11. Experimental setup for 2-point probe resistivity measurement.

4.3.3 Results and Discussions

4.3.3.1 SEM Characterization

During evaporation of the DNA buffer solution, the DNA is tethered on the glass substrate and stretched along the receding meniscus. Figure 4.12 shows a schematic of the DNA stretching mechanism during the evaporation process. SEM micrograph of DNA coated glass substrate (control) is shown in Figure 4.13. The control acts as a reference for comparison with the metal deposited samples. The image can be interpreted as bundle of CT DNA strands branching out in different directions.
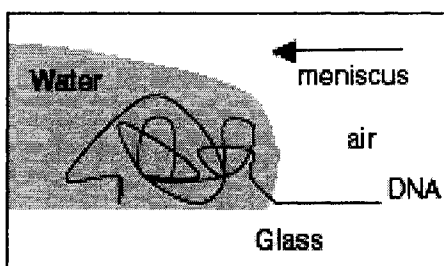
Figure 4.12 Mechanism of DNA stretching by evaporation.
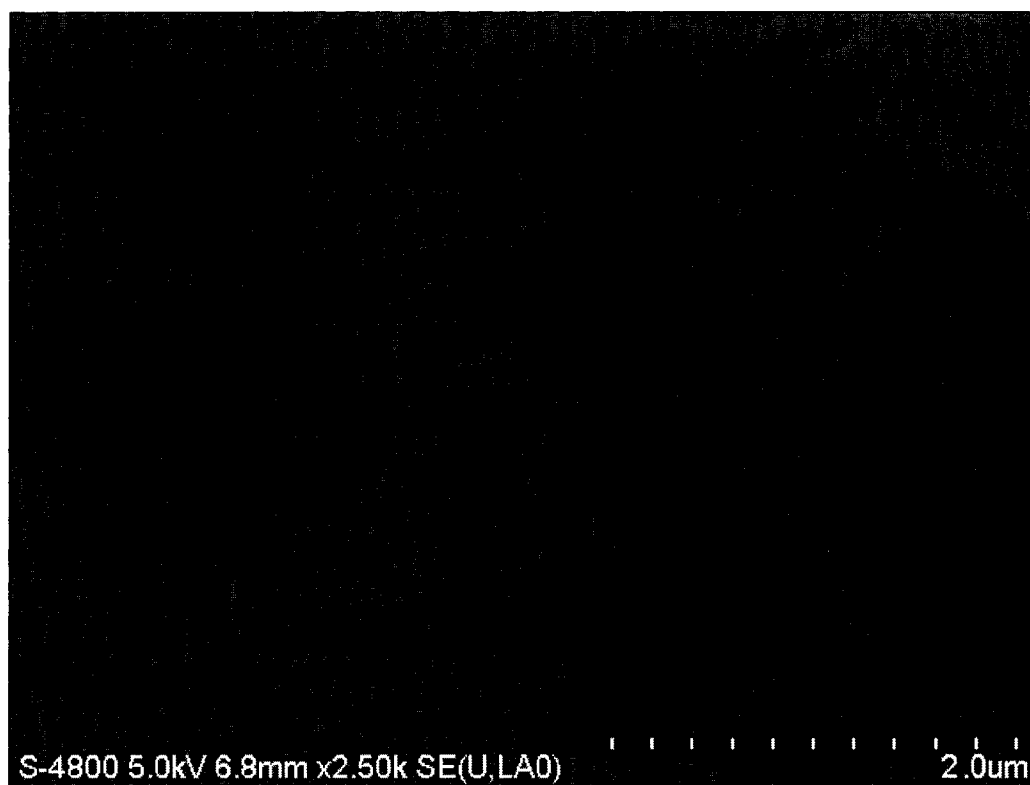
Figure 4.13 SEM micrograph of stretched DNA (control).

An SEM image of untreated metallized DNA sample is shown in Figure 4.14. Deposition of indium(0) in the form of indium nanoparticles on immobilized DNA strands could be observed. Higher concentration of nanoparticle deposition on the DNA was found along the evaporated edge of the meniscus and metal deposition on the glass

substrate was minimal. Considerable irregularity and roughness along the length of the

nanowires was also visible in the SEM image.
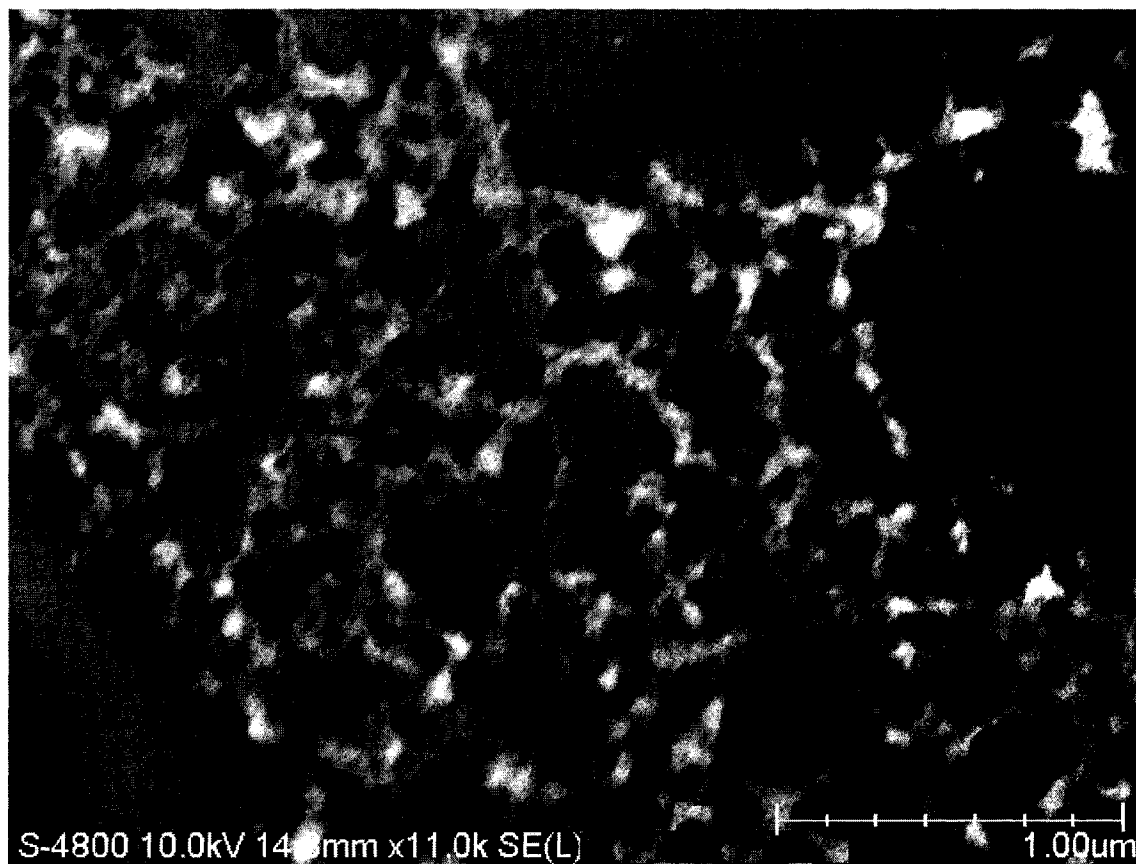
Figure 4.14 SEM micrograph of untreated metallized DNA
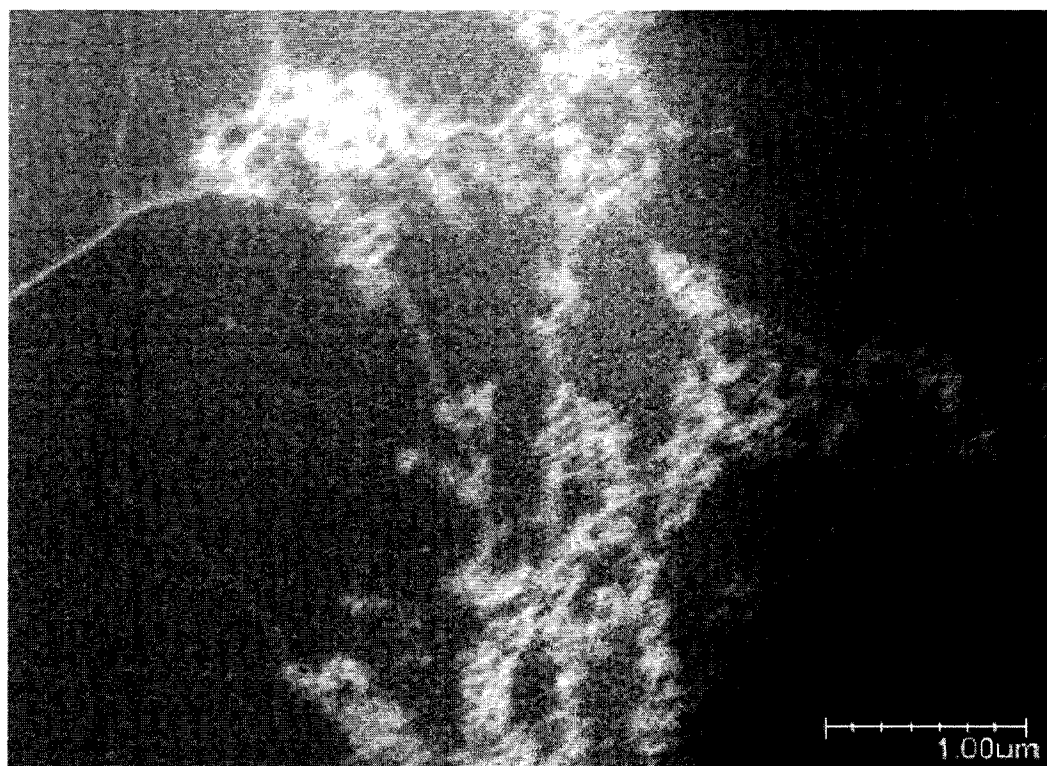
Figure 4.15. SEM micrograph of heat treated metallized DNA.

The effect of heat treatment on metallized DNA can be observed in the SEM image shown in Figure 4.15. The figure however, is a representative of the entire sample and not the same region imaged for the untreated metallized DNA. It can be observed that the irregularity and roughness along the length of the DNA strands has been significantly reduced due to the heat treatment process. However, aggregation and fusion of adjacent nanowires was also observed.

4.3.3.2 Electrical Characterization

Results for preliminary surface resistivity measurements are tabulated in Table 4.1. Our control surfaces, glass and DNA had an average resistivity of 5.37×10^{13} mΩ and 1.74×10^{13} respectively. Average resistivity for untreated metallized DNA surface $(1.83 \times 10^{10}$ m$\Omega)$ and heat-treated metallized DNA surface $(3.39 \times 10^{9}$ m$\Omega)$ were

relatively low. This result implies that in this case heat treatment has reduced the resistivity by a factor of 5. However, these resistivity measurements are preliminary and need further investigation. The observed high resistivity of both untreated and heat-treated metallized DNA surface is due the discontinuity of the nanowires and the contact resistance between the probe and the nanowires.

Table 4.1. Electrical resistivity data

Test region	Glass substrate (control) $(m\Omega)$	DNA (control) $(m\Omega)$	Untreated Metallized DNA $(m\Omega)$	Heat treated metalized DNA $(m\Omega)$
1	2.80×10^{13}	1.35×10^{13}	4.30×10^{10}	8.81×10^{8}
2	2.20×10^{13}	2.90×10^{13}	7.60×10^{9}	5.59×10^{9}
3	1.11×10^{14}	9.70×10^{12}	4.28×10^{9}	3.70×10^{9}

4.4 Sodium Reduced Indium Nanoparticles-DNA Interaction Studies

4.4.1 Materials and Method

Several 40X dilute solutions of indium nanoparticles from sodium reduction of InCl in toluene (Section 3.4.1) were used. Indium nanoparticles solution from sodium reduction of InCl (5 μL) was pipetted on the DNA coated glass substrate. The solution was allowed to dry under a fume hood of 30 min and then dried by passing nitrogen gas over it. The sample was sputtered with 4 nm gold layer and imaged under SEM.

4.4.2 Results and Discussions

The medium used for dispersing the indium nanoparticles was toluene. Evaporation of the solvent occurred within 15 min of pipetting. No definite evidence of metal deposition on DNA was found in the sample. SEM image shows random distribution of agglomerated indium nanoparticles (Figure 4.14). Presence of DNA could not be verified by imaging. However, the features in Figure 4.14 can be interpreted as non-specific metal deposition on and around DNA molecules.

Figure 4.14 SEM micrograph of indium nanoparticles from sodium reduction of InCl deposited   on   DNA

CHAPTER 5

CONCLUSIONS AND FUTURE WORK

5.1 Conclusions

In this project, a "bottom-up" approach of manufacturing involving manipulation of basic building blocks of matter to achieve desired shape and size is investigated. This approach mainly involves fabricating metal nanowires using DNA molecules as template and indium species as the basic building block. The work here can provide the fundamental knowledge for developing fabrication techniques that provides cheaper and more accurate techniques to replace current technology based on optical lithography. The longterm goal of this project is to achieve self-assembling conducting nanowires as electrical interconnects with resistively close to that of bulk metal (indium, in this case). The accomplishments of our project are described in the following paragraphs.

This project started with an investigation into the interaction of indium (III), indium(I) and indium(0) with DNA in the process of DNA metallization in order to study the role of these indium species in the formation of DNA templated indium nanowires.

First, an aqueous solution of trivalent indium salt ($InCl_3$) was used to investigate In(III)-DNA interactions. Based on spectroscopic, fluorescence and gel electropherosis techniques we used for indium(III)-DNA binding studies, following conclusions were reached: 1) indium(III) ions bind to DNA molecules in aqueous solution, leading to a

75

significant change in spectral and extrinsic fluorescence properties of DNA; 2) indium-bound DNA has a higher melting point than free DNA; 3) EDTA affects indium(III) ions bound to the DNA molecules by chelation in aqueous solution, reversing the conformational changes that occurred by increased concentration of In(III); 4) indium(III) ions induce considerable aggregation and condensation of DNA molecules, leading to bundling and coiling of DNA.

Second, we have studied the *in situ* sodium reduction of indium(I) complex on DNA molecules using SEM. DNA templated indium nanowires hence obtained were heat treated and a preliminary investigation on electrical resistivity was conducted. NMR spectroscopy was used to characterize the indium(I) complex used as precursor for DNA metallization. Following conclusions were reached based on the above studies: 1) monoatomic indium(I) ions are highly air sensitive but can be stabilized by incorporating indium(I) ion in a suitable organic coordination complex; 2) pyrazole ligand with bulky group such as phenyl exhibits much greater steric hinderance (stability) in the complex as compared to cyclopentadienyl complexes; 3) *in situ* sodium reduction of indium(I) complex, [HB(3-phpz)₃]In to indium(0) on DNA immobilized substrate produces deposition of indium(0) specifically on the DNA strands; 4) indium(I) ions bound to DNA are reduced by sodium to In(0) forming nucleation sites for further electroless deposition of In(0) on the DNA strands; 5) irregularity and roughness along the length of the DNA nanowires can be reduced by subsequent heating and annealing making the wires relatively smooth; 6) heating the nanowires to the melting point of indium and subsequent annealing could reduce the resistivity of the nanowires by a factor of 5; 7)

high resistivity of the nanowires is due to the discontinues structure of the wires and high contact resistance between nanowire surface and the test probe.

Third, we have investigated the direct deposition of indium(0) in the form of indium nanoparticles as a method of DNA templated nanowire assembly. First, indium nanoparticles were synthesized by the following three methods: 1)sodium reduction of indium(I) chloride; 2) sodium reduction of indium complex ([HB(3-phpz)$_3$]In); 3) dispersion of bulk indium in mineral oil. Then, the nanoparticles were deposited directly on DNA molecules immobilized on glass substrate. Based on SEM and EDX characterizations, following conclusions were reached: 1) indium nanoparticles prepared from sodium reduction of InCl and {[HB(3-phpz)$_3$]In} have diameters in 10-100 nm range and were distributed uniformly; 2) composition of indium in the indium nanoparticles prepared from sodium reduction of InCl and {[HB(3-phpz)$_3$]In} is relatively low (25-50% by weight); 3) indium nanoparticles synthesized by dispersion of bulk indium in mineral oil have relatively large particle size and irregular particle size distribution; 4) composition of indium in indium nanoparticles synthesized by dispersion of bulk indium in mineral oil is relatively high (85% by weight); 5) direct deposition of indium nanoparticles prepared by sodium reduction of indium(I) chloride, on DNA strands immobilized on a glass substrate produced random distribution of agglomerated indium nanoparticles; 6) indium nanoparticles do not deposit specifically on DNA strands.

Even though indium(III) have confirmed affinity towards DNA molecules, condensation and coiling of DNA molecules in presence of indium(III) ions will make it difficult to maintain stretched and aligned DNA molecules during metallization process.

A former member of our research group had shown [107] that reduction of immobilized DNA-bound indium(III) ions using p-dimethylaminobenzaldehyde (DMAB) produces aggregated clusters of metallized DNA. However, specific deposition of indium(0) on DNA was observed. Hence, we adopted direct deposition of indium(0) on immobilized DNA to prevent aggregation and coiling. Direct deposition method however lacked the specificity of deposition. Based on our experiments with the three indium species, we conclude that *in situ* sodium reduction of {[HB(3-phpz)₃]In} in the presence of DNA is the most suitable method for the assembly of DNA templated indium nanowires.

5.2 Future Work

In this work, we have partially accomplished the long term goals of the project. Further improvements in precursor synthesis, DNA stretching and alignment process and the DNA metallization process is required to develop highly reliable and cost effective interconnects for futuristic nanocircuits.

Synthesis of {[HB(3-phpz)₃]In} is a long process and several steps are highly critical requiring intense care. Development of a more efficient synthetic route is important to provide a cost effective solution when commercialization is required. DNA with thiol modified ends can be stretched across gold microelectrodes before indium deposition. Metallized DNA can then be heated and annealed in vacuum (or inert atmosphere) to obtain smoother structure. This method will eliminate discontinuity and contact resistance, providing an ideal setup for electrical characterization. Detailed study of electrical characteristics and temperature dependence will reveal the performance of the nanowires under device conditions.

Future holds enormous possibilities for low temperature DNA-templated metal nanowires. For controlling the orientation and length of the DNA-templated nanowires in the required position inside the nanocircuits, manipulation of DNA molecules on the circuit surface is required prior to further processing. Individual DNA molecules must be synthesized with specific number of base pairs, separated, and stretched between specific electrodes in the circuit to serve as templates for nanowire fabrication. Thus, DNA can be positioned in nanocircuits with high precision by molecular recognition and metallized *in situ*. Interconnects thus obtained can be heated and annealed to eliminate any structural defects thus enhancing their conductivity. Such interconnects have potential to exhibit high performance and can operate at single-molecule level connecting various components in nanocircuits.

APPENDIX

SYNTHESIS PROCEDURE DESCRIPTIONS AND NMR SPECTRA

80

A. Procedure for drying solvents using sodium and benzophenone

1) Place the solvent in a round bottom flask with magnetic stir bar in it. Add freshly cleaved sodium (~5 g per 100 mL) and benzophenone (10 g per 100 mL). Do not use more than 50% of the volume of the flask.

2) Connect round bottom flask to water cooled condenser. Attach nitrogen supply and oil trap to the condenser. Adjust nitrogen supply so that the gas bubbles regularly out of the oil trap.

3) Place the heating mantle and magnetic stirrer under the round bottom flask. Set heat just over boiling point of the solvent. Solvent should condense in the condenser and return to the flask. Allow the solvent to reflux for ~24 h.

4) Make sure that the solvent has turned dark purple in color. Connect Schlenk flask to the side arm of the condenser and collect the distilled solvent.

5) Close the stopcock of the Schlenk flask. The solvent is ready to use.

B. Procedure for degassing of liquids using Freeze-Pump-Thaw method

1) Place the solvent (or solution) in a Schlenk flask. Make sure the stopcock is closed. Do not use more than 50% of the volume of the flask to avoid cracking of the flask during the procedure.

2) Connect the Schlenk flask to the vacuum line and freeze the liquid using liquid nitrogen filled dewar.

3) Open the stopcock to vacuum and pump down the flask after the solvent is frozen (~ 1h).

4) Close the stopcock to seal the flask.

5) Thaw the solvent until it just melts using a tepid water bath. Gas bubbles should evolve from the solution. Do not over heat or shake the flask.

6) Replace the water bath with the liquid nitrogen filled dewar and refreeze the solvent.

7) Repeat steps (3) – (7) until evolution of gas during thawing ceases. The solution should be put through a minimum of three cycles.

8) The solvent can be transferred through distillation for use.

C. Protocol for purification of CT DNA (QIAEX II Handbook)

QIAEX II Gel Extraction Kit can be used to purify and concentrate DNA fragments from 40 bp to 50 kb from aqueous solutions without phenol extraction or ethanol precipitation. Purification of DNA fragments with the QIAEX II system is based on solubilization of agarose and selective adsorption of nucleic acids onto QIAEX II silica-gel particles in the presence of chaotropic salt. QIAEX II separates DNA from salts, agarose, polyacrylamide, dyes, proteins, and nucleotides without phenol extraction or ethanol precipitation.

1)   Add ethanol (96–100%) to Buffer PE before use.

2)   All centrifugation steps are at maximum speed ($\geq$10,000 x g, ~13,000 rpm) in a conventional table-top microcentrifuge.

3)   For DNA fragments larger than 10 kb, mix by gently flicking the tube to avoid shearing the DNA. Do not vortex the tube.

4)   Transfer the sample to a colorless tube. Add 3 volumes of Buffer QX1 to 1 volume of sample.

5)   Add 3 volumes of Buffer QX1 plus 2 volumes of H_2O.

6)   Check that the color of the sample mixture is yellow. If the color of the mixture is orange or purple, add 10 μL 3M sodium acetate, pH 5.0, and mix. The color should now be yellow. The adsorption of DNA to QIAEX II particles is only efficient at pH $\leq$7.5. Buffer QX1 now contains a pH indicator which is yellow at pH $\leq$7.5, and orange or violet at higher pH, allowing easy determination of the optimal pH for DNA-binding.

7) Resuspend QIAEX II by gentle flicking for 30 sec.

8) Add 10 μL of QIAEX II per 5 μL of DNA and mix. Incubate at room temperature for 10 min. Mix every 2 min to keep QIAEX II in suspension.

9) Centrifuge the sample for 30 sec and remove supernatant.

10) Wash the pellet twice with 500 μL of Buffer PE.

11) Air-dry the pellet for 10–15 min or until the pellet becomes white. Do not vacuum dry, as this may cause overdrying. Overdrying the QIAEX II pellet may result in decreased elution efficiency.

12) To elute DNA, add 20 μL of 10 mM Tris-Cl, pH 8.5, or H_2O and resuspend the pellet by gentle flicking. Incubate at 50°C for 10 min.

13) Centrifuge for 30 sec. Carefully transfer the supernatant into a clean tube. The supernatant now contains pure DNA.

14) Centrifuge for 30 sec. Carefully transfer the supernatant into a clean tube. The supernatant now contains pure DNA.

15) Repeat steps 12 and 13 and combine the eluates. A second elution step will increase the yield by approximately 10–15%.
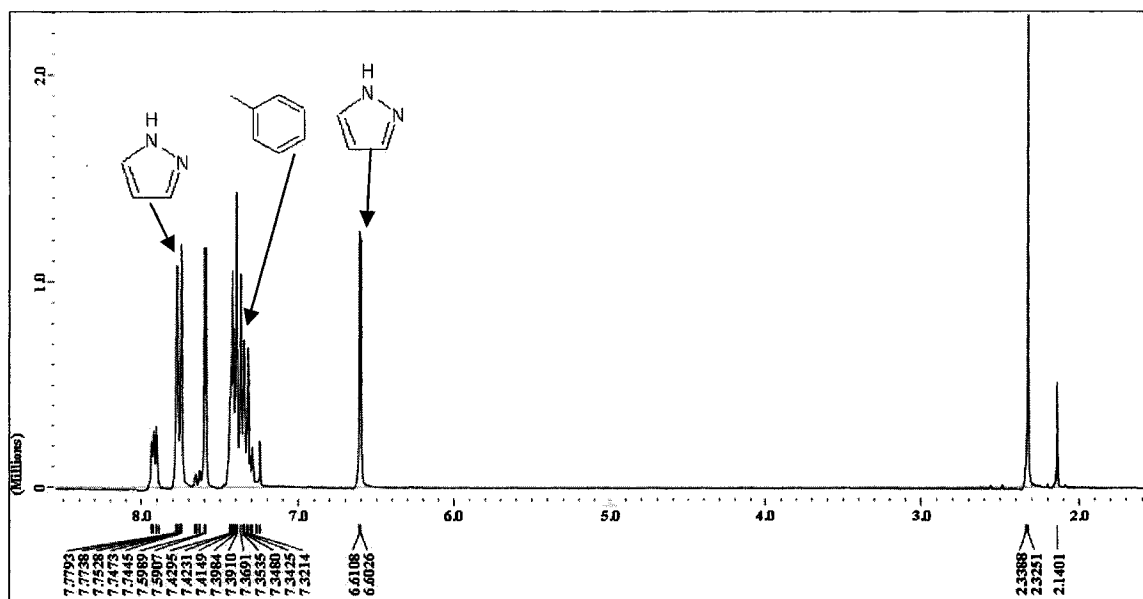
D. NMR Spectra

Figure 1 ¹H NMR spectrum for 3-phenylpyrazol. Peaks specific to phenyl and pyrazol group is indicated.

Figure 2. ¹³C-Couple NMR spectrum for 3-phenylpyrazol. Peaks specific to phenyl and pyrazol group is indicated.
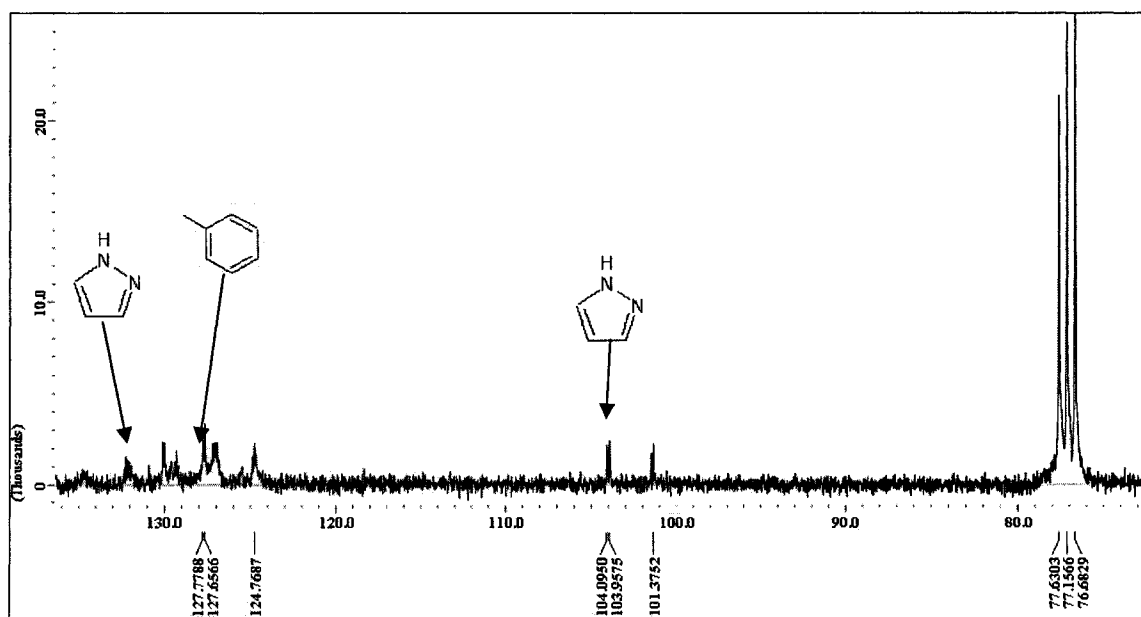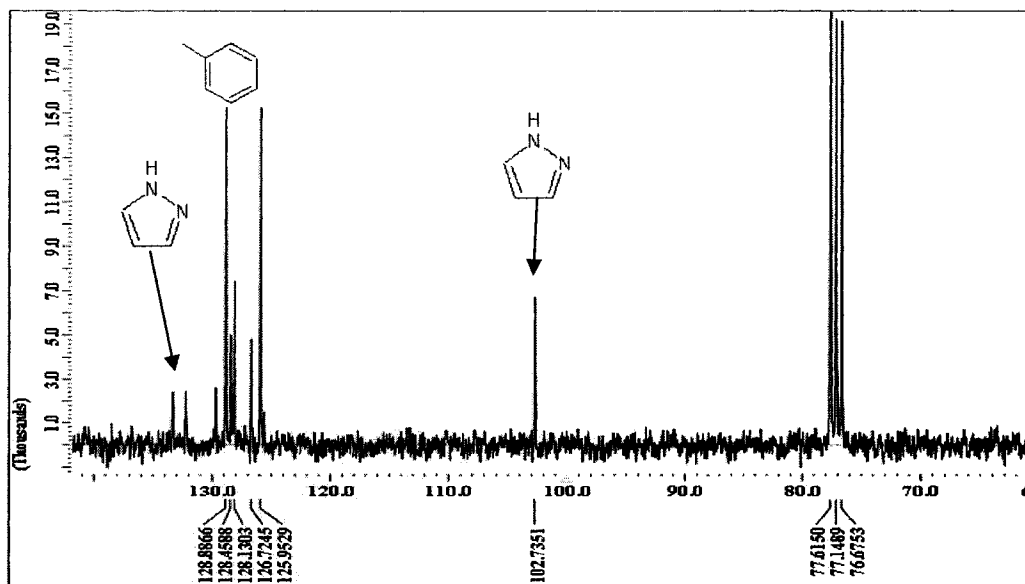
Figure 3. ^{13}C-Decouple NMR spectrum for 3-phenylpyrazol. Peaks specific to phenyl and pyrazol group is indicated.
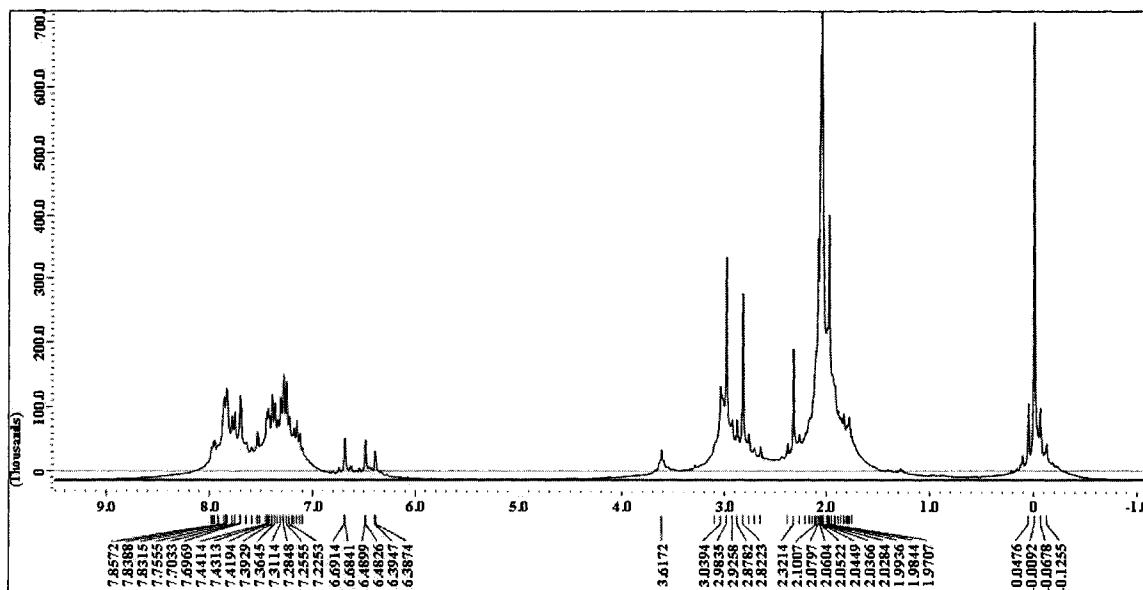
Figure 4. ^{1}H NMR spectrum for $KH_2B(3\text{-phpz})_2$
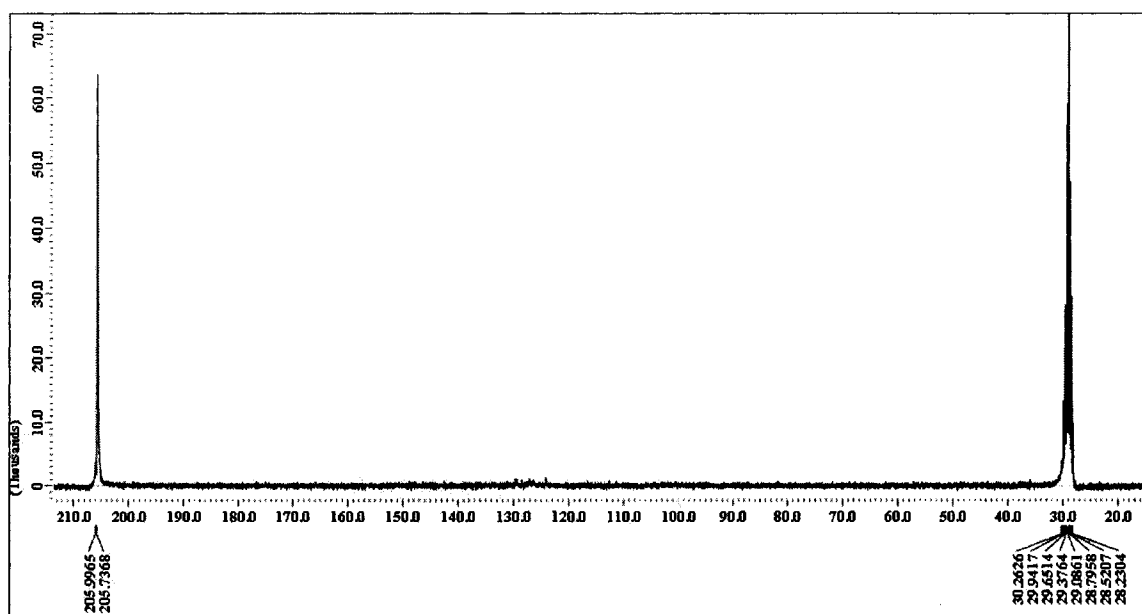
Figure 5. ^{13}C-Couple NMR spectrum for KH$_2$B(3-phpz)$_2$
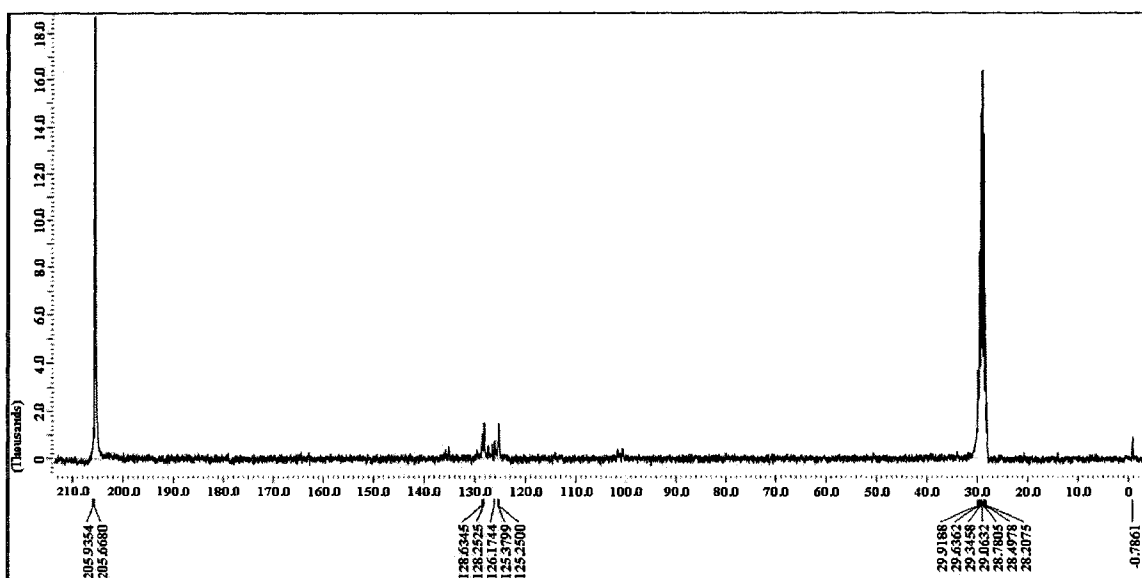
Figure 6. ^{13}C-Decouple NMR for KH$_2$B(3-phpz)$_2$
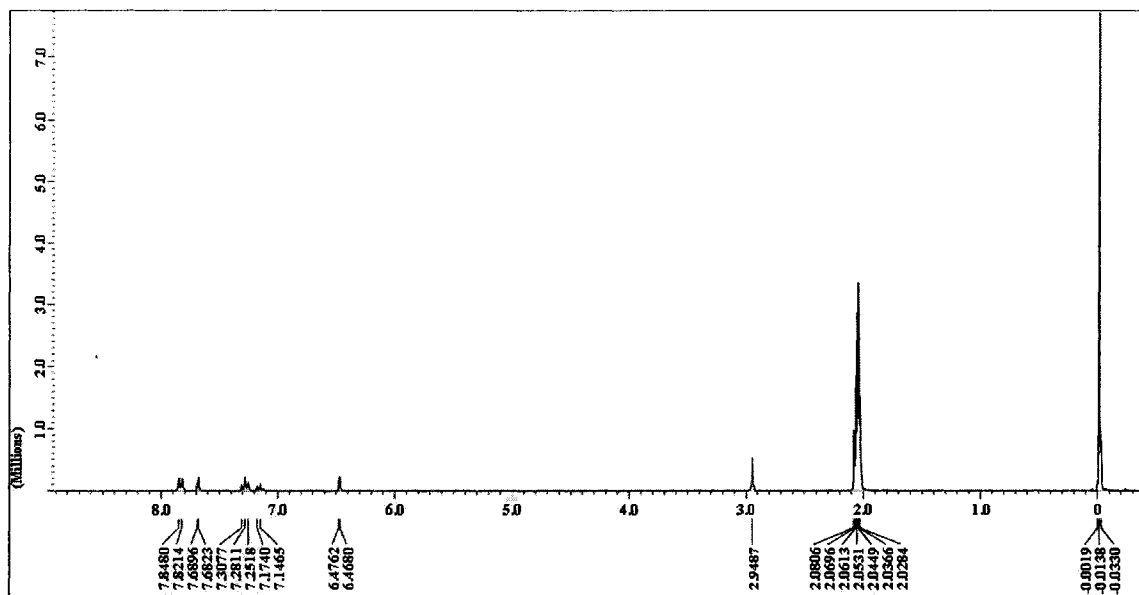
Figure 7. ^{1}H NMR spectrum for KHB(3-phpz)$_3$
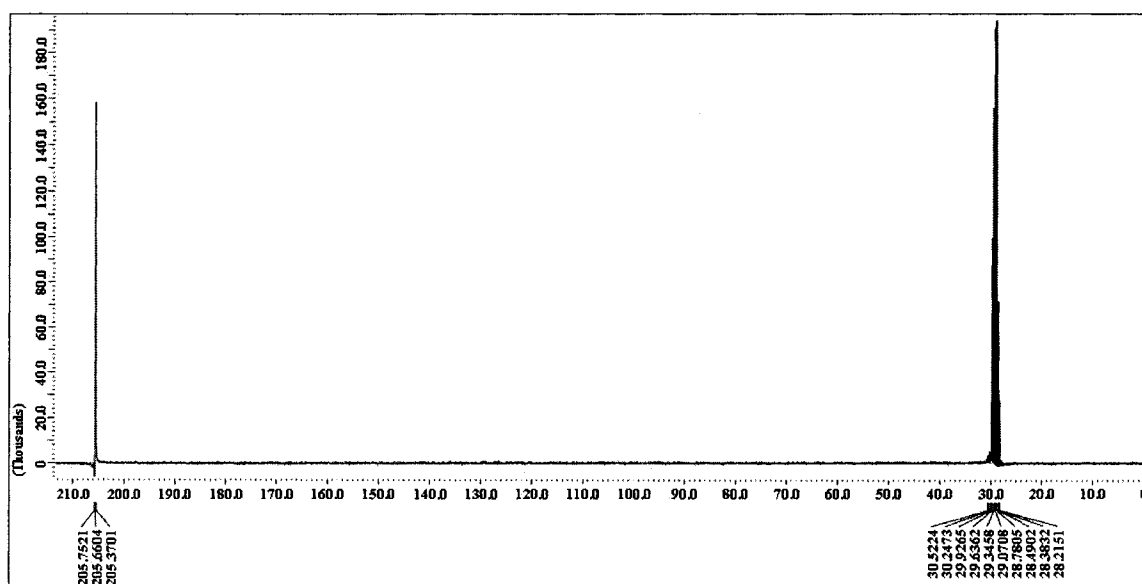
Figure 8. ^{13}C-Couple NMR spectrum for KHB(3-phpz)$_3$
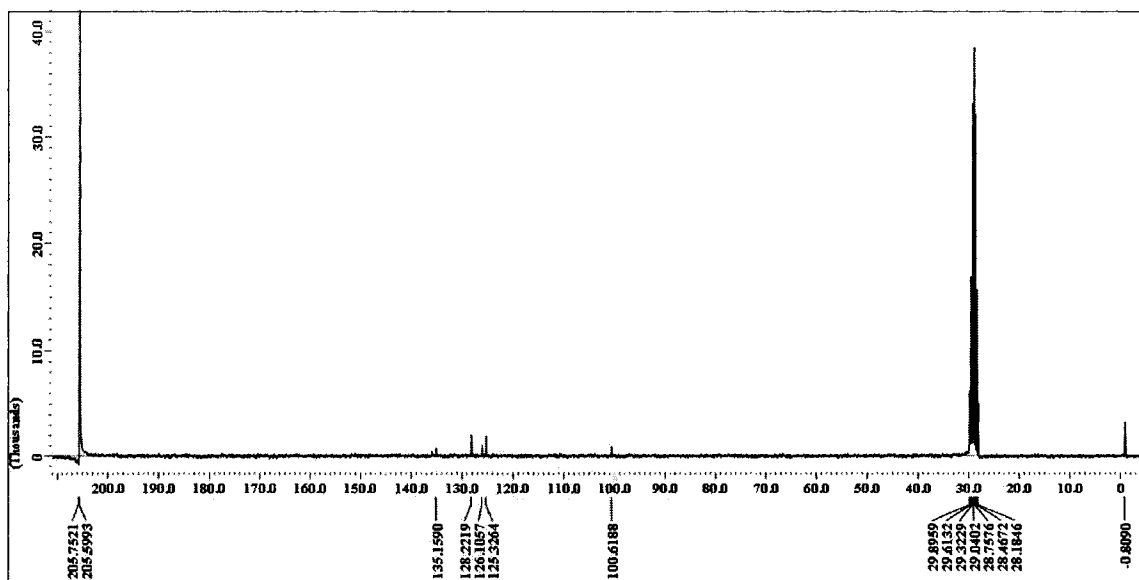
Figure 9. ^{13}C-Decouple NMR spectrum for KHB(3-phpz)$_3$
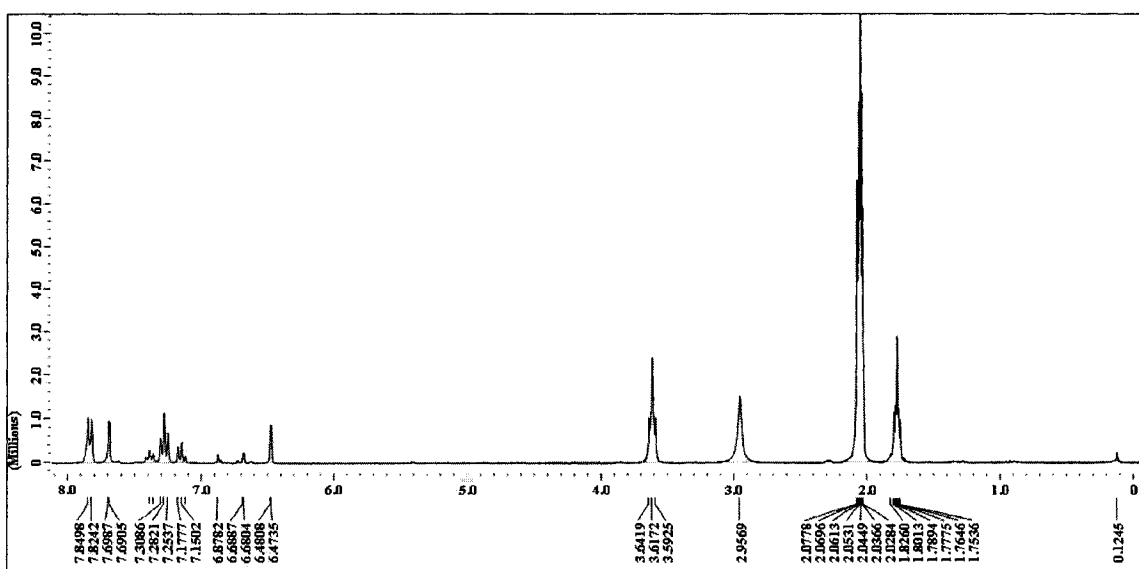
Figure 10. ^{1}H NMR spectrum for [HB(3-phpz)$_3$]In
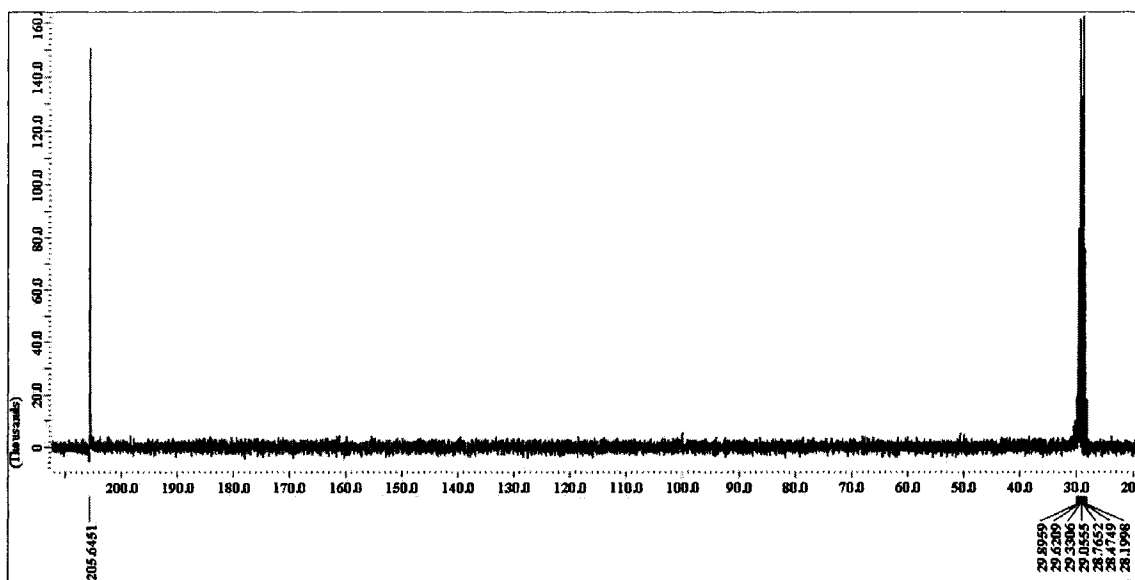
Figure 11. ^{13}C-Couple NMR spectrum for [HB(3-phpz)$_3$]In
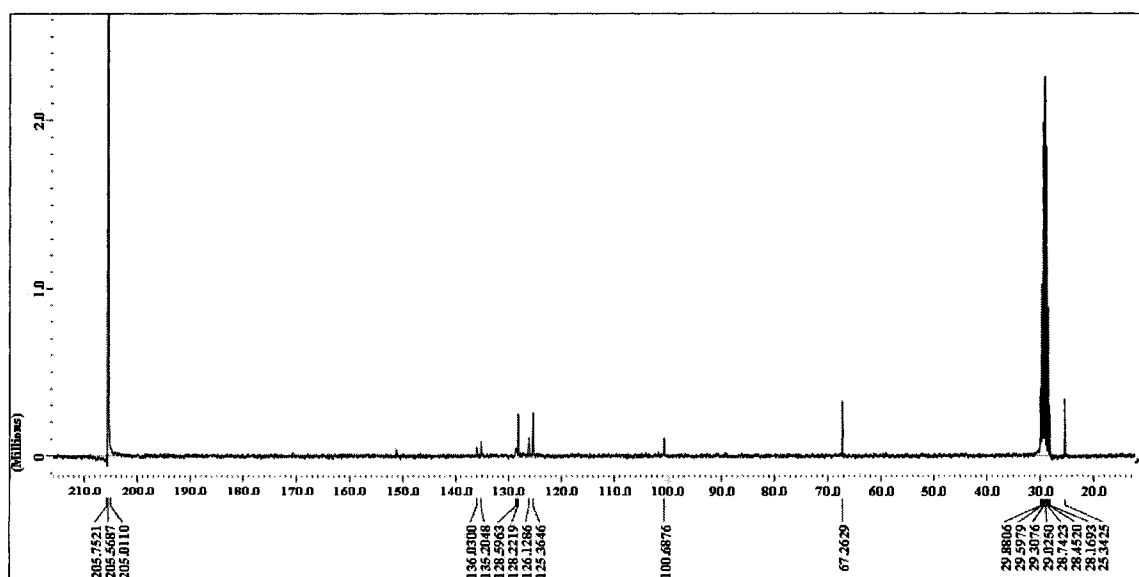
Figure 12. ^{13}C-Decouple NMR spectrum for [HB(3-phpz)$_3$]In

REFERENCES

[1]   Willard G. Christopher, J. Wu, M. Eastwood, A. Snell, "Intel Brings Dual-Core Capabilities to Itanium 2 with Montecito Processor," *Manufacturing Insights*, 2006.

[2]   P. J. Silverman, "The intel lithography roadmaps," *Intel Tech. J.*, **6** 55 2002.

[3]   The 2004 international roadmap for semiconductors (ITRS), 2004.

[4]   M. C. Raco, "The future of the nantional nanotechnology initiative," *www.nano.gov/html/res/slides.pdf*, 2003.

[5]   Y. Cui,X. Duan, J. Hu, C. M. Liebe, "Doping and Electrical Transport in Silicon Nanowires," *J. Phys. Chem. B*, **104** 5213 2000.

[6]   Y. Cui, Z. Zhong, D. Wang, W. U. Wang, C. M. Lieber, "High performance silicon nanowire field effect transistors," *Nano Lett.*, **3** 149 2003.

[7]   A. B. Greytak, J. L. Lauhon, M. S. Gudiksen, C. M. Liebera, "Growth and transport properties of complementary germanium nanowire field-effect transistors," *App. Phys. Lett.*, **84** 4176 2004.

[8]   Z. Zhong, F. Qian, D. Wang, C. M. Lieber, "Synthesis of p-type gallium nitride nanowires for electronic and photonic nanodevices," *Nano Lett.*, **3** 343 2003.

[9]   N. P. Guisinger , M. E. Greene, R. Basu, A. S. Baluch, M. C. Hersam, "Room temperature negative differential resistance through individual organic molecules on silicon surface," *Nano Lett.*, **4** 55 2004.

[10]   A. S. Blum, J. G. Kushmerick, D. P. Long, C. H. Patterson, J. C. Yang, J. C. Henderson, Y. Yao, J. M. Tour, R. Shashidhar, B. R. Ratna, "Molecularly inherent tage controlled conductance switching," *Nature Mater.*, **4** 167 2005.

[11]   C. L. Curtis, J. E. Ritchie, M. J. Sailor, "Fabrication of conducting polymer interconnects," *Science*, **262** 2014 1993.

[12]   Y. Xia and P. Yang, "Guest Editorial: Chemistry and Physics of Nanowires," *Adv. Mater.*, **15**, 351 2003.

[13] K. W. Kolasinski, "Catalytic growth of nanowires: Vapor-liquid-solid, vapor-solid-solid, solution-liquid-solid and solid-liquid-solid growth," *Curr. Opin. Solid State Mater. Sci.*, **10** 192 2006.

[14] M. Z. Atashbar and S. Singamaneni, " Template-based fabrication of metal nanostructures," *Proc. Inst. Mech. Eng., Part N: J. Nanoeng. Nanosys.*, **218** 83 2004.

[15] K. Tang, Y. Qian, J. Zheng, X. Yang, "Solvothermal route to semiconductor nanowire," *Adv. Mater.*, **15** 448, 2003.

[16] Y. Ito and E. Fukusaki, "DNA as a 'Nanomaterial'," *J. Mol.Cat. B: Enzy.*, **28** 155 2004.

[17] E. Gazit, "Use of biomolecular templates for the fabrication of metal nanowires," *FEBS J.*, . **274** 317 2007.

[18] G. B. Onoa ,G. Cervantes, V. Moreno, M. J. Prieto, "Study of the interaction of DNA with cisplatin and other Pd(II) and Pt(II) complexes by atomic force microscopy," *Nucleic Acids Res.*, **26** 1473 1995.

[19] J. Duguid, V. A. Bloomfield, J. Benevides, G. J. Thomas, "Raman spectroscopy of DNA–metal complexes. I. Interactions and conformational effects of the divalent cations: Mg, Ca, Sr, Ba, Mn, Co, Ni, Cu, Pd, and Cd," *Biophys. J.*, **65** 1916 1993.

[20] E. Braun, Y. Eichen, U. Sivan, G. Ben-Yoseph, "DNA-templated assembly and electrode attachment of a conducting silver wire," *Nature*, **39** 775 1998.

[21] J. Richter, M. Mertig, W. Pompe, I. Mönch, H. K. Schackert, "Construction of highly conductive nanowires on a DNA template," *Appl. Phys. Lett.*, **78** 536 2001.

[22] J. Richter, R. Seidel, R. Kirsch, M. Mertig, W. Pompe, J. Plaschke, H. K. Schackert, "Nanoscale palladium metallization of DNA," *Adv. Mater.*, **12** 507 2000.

[23] J. Richter, M. Mertig, W. Pompe, H. Vinzelberg, "Low-temperature resistance of DNA-templated nanowires," *Appl. Phys. A*, **74** 725 2002.

[24] W. E. Ford, O. Harnack, A. Yasuda, J. M. Wessels, "Platinated DNA as precursors to templated chains of metal nanoparticles," *Adv. Mater*, **13** 1793 2001.

[25] R. Seidel, M. Mertig, W. Pompe, "Scanning force microscopy of DNA metallization," *Surf. Interface Anal.*, **33** 151 2002.

[26]   R. Seidel, L. C. Ciacchi, M. Weigel, W. Pompe, M. Mertig, "Synthisis of platinum cluster chains on DNA templates:conditions for template-controlled cluster growth," *J. Phys. Chem. B*, **108** 10801 2004.

[27]   A. Kumar, M. Pattarkine, M. Bhadbhade, A. B. Mandale, K. N. Gamesh, S. S. Datar, C. V. Dharmadhikari, M. Shastry, "Linear superclusters of colloidal gold particles by electrostatic assembly on DNA templates," *Adv. Mater.*, **13** 341 2001.

[28]   M. Shastry, A. Kumar, S. S. Datar, C. V. Dharmadhikari, K. N. Gamesh, "DNA-mediated electrostatic assembly of gold nanoparticles into linear arrays by a simple drop-coating procedure," *Appl. Phys. Lett.*, **78** 2943 2001.

[29]   C. J. Loweth, W. B.Caldwell, X. Peng, A. P. Alivisatos A P, P. G. Schultz, "DNA-based assembly of gold nanocrystals," *Angew. Chem. Int. Edn*, **38** 1808 1999.

[30]   C. Cheng, Q. Gu, R. K. Gonela, D. T. Haynie, "Self-Assembly of metallic nanowires from aqueous solution," *Nano. Lett.*, **5** 175 2005.

[31]   B. A. Cook, I. E. Anderson, J. L. Harringa, R. L. Terpstra, "Effect of heat treatment on the electrical resistivity of near-eutectic Sn-Ag-Cu Pb-free solder alloys," *J. Elec. Mater.*, **31** 1190 2002.

[32]   W. G. Haines and R. H. Bube, "Effects of heat treatment on the optical and electrical properties of indium–tin oxide films," *J. Appl. Phys.*, **49** 304 1978.

[33]   H. Kudo and M. Fujihira, "DNA-Templated copper nanowire fabrication by a two-Step process in ving electroless metallization," *IEEE Trans. Nanotech.*, **5** 90 2006.

[34]   K. Keren, R. S. Berman, E. Braun, "Patterned DNA Metallization by Sequence-Specific Localization of a Reducing Agent," *Nano. Lett.*, **4** 323 2004.

[35]   J. Kleinberg, *Inorganic Chemistry*. Boston: Heath, 1960.

[36]   K.J. Lee and T.L. Brown, "Ligand steric properties," *Coord. Chem. Rev*, **128** 89 1993.

[37]   A.D. Garnovskii and B.I. Kharissov, *Synthetic Coordination and Organometallic Chemistry*. Marcel Dekker, 2003.

[38]   I. J. McColm and P. L. Goggin, "Lower valent indium compounds - Some studies in complex formation," *J. Inorg. Nucl. Chem*, **28** 2501 1966.

[39] T. P. Radhakrishnan and A. K. Sundaram, "A polarographic study of indium thiocyanate complexes," *J. Electroanal. Chem.*, **5** 124 1963.

[40] T. Douglas, K. H. Theopold, B. S. Haggerty, A. L. Rheingold, "A phospholyl complex of indium," *Polyhedron*, **9** 329 1990.

[41] S. Ghoshal, V. K. Jain, D. P. Dutta, P. P. Phadnis, M. Nethaji, "Gallium and indium dithiocarboxylates: synthesis, spectroscopic characterization and structure of [MeGa(S$_2$Ctol)$_2$]," *J. Organomet. Chem.*, **691** 5838 2006.

[42] D. G. Tuck and J. S. Poland, "Coordination compounds of indium - XIII. Tricyclopentadienylindium(III) and some related compounds," *J. Organomet. Chem.*, **42** 307 1972.

[43] D. L. Reger, "Poly(pyrazolyl) borate complexes of gallium and indium," *Coord. Chem. Rev*, **147** 571 1996.

[44] M. Figuet, M. T. Averbuch-Pouchot, A. M. d'Hardemare, O. Jarjayes, "Tripodal Iminophenolate Ligand Complexes of Gallium(III), Indium(III), and Thallium(III)," *Eur. J. Inorg. Chem.*, **2001** 2089 2001.

[45] P. C. Kuo, J. H. Huang, C. H. Hung, G. H Lee and S. M. Peng, "Synthesis and Characterization of Five-Coordinate Gallium and Indium Complexes Stabilized by Tridentate, Substituted Pyrrole Ligands,'" *Eur. J. Inorg. Chem.*, **2003** 1440 2003.

[46] C. Üeffing, A. Ecker, R. Koeppe, H. Schnoeckel, "Synthesis, structure, and bonding of a polyhedral Al$_2$Co$_2$ cluster," *Organometallics*, **17**. 2373 1998.

[47] W. Ziemkowska and R. Anulewicz-Ostrowska, "Sterically crowded diolates of group 13 metals," *J. Organomet. Chem.*, **689** 2056 2004.

[48] Jr. O. T. Beachly, J. C. Pazlk, T. E. Glassman, M. R. Churchill, J. C. Fettinger and R. Blom, "Synthesis, characterization, and structural studies of In(C$_5$H$_4$Me) by X-ray diffraction and electron diffraction techniques and a reinvestigation of the crystalline state of In(C$_5$H$_5$) by X-ray diffraction studies," *Organometallics*, **7** 1051 1988.

[49] E. O. Fischer and H. P. Hofmann, "Metall-cyclopentadienyle des Indiums," *Angew. Chem.*, **69** 639 1957.

[50] C. Peppe, D. G. Tuck, L. Victoriano, "A simple synthesis of cyclopentadienylindium(I)," *J. Chem. Soc., Dalton Trans.*, **12** 2592 1981.

[51] S. Trofimenko, "Boron-Pyrazole Chemistry," *J. Am. Chem. Soc.*, **88** 1842 1966.

[52] S. Trofimenko, *Scorpionates: The Coordination Chemistry of Polypyrazolyborate Ligands*. London: Imperial College Press, 1999.

[53] R. Mukherjee, "Coordination chemistry with pyrazole-based chelating ligands: molecular structural aspects," *Coord. Chem. Rev.*, **203** 151 2000.

[54] A. Frazer, B. Piggott, M. Harman, M. Mazid, M. B. Hursthouse, "Synthesis and X-Ray crystal structures of [bis{(3,5-Dimethylpyrazolyl)₃Hydridoborato}In]I and [bis{(pyrazolyl)₃methylgallato} In][InI₄]," *Polyhedron*, **11** 3013 1992.

[55] A. Frazer, B. Piggott, M. B. Hursthouse, M. Mazid, "Synthesis and crystal and molecular structure of [(hydroboratotris(3'-phenylpyrazolyl))indium]: an air-Stable monomeric Indium(1) complex," *J. Am. Chem. Soc.*, **116** 4127 1994.

[56] S. Trofimenko, J. C. Calabrese, P. J. Domaille, J. S. Thompson, "Steric effects in polypyrazolylborate ligands. poly(3-isopropylpyrazolyl)borates: ligands of intermediate steric requirements," *Inorg. Chem.*, **28** 1091 1989.

[57] S. Trofimenko, J.C. Calabrese, J.S. Thompson, "Novel polypyrazolylborate ligands: coordination control through 3-substituents of the pyrazole ring," *Inorg. Chem.*, **26** 1507 1987.

[58] R. M. Claramunt, M. D. Santa María, I. Forfar, F. A. Parrilla, M. Minguet-Bonvehí, O. Klein, H. Limbach, C. Foces-Foces, A. L. Llamas Saiz, J. Elguero, "Molecular structure and dynamics of C-1-adamantyl substituted N-unsubstituted pyrazoles studied by solid state NMR spectroscopy and X-ray crystallography," *J. Chem. Soc., Perkin Trans. 2*, . 1997, pp. 1867, 1997.

[59] W. L. F. Armarego, *Purification of Laboratory Chemicals*, 4 ed: Elsevier, 2003.

[60] R. Jacquier J. Elguero, "Synthesis of aryl substituted pyrazoles," *Bull. Soc. Chim. Fr.*, **1966** 13 1966.

[61] P. Holister, J.W. Weener, C.R. Vas, T. Harper, "Nanoparticles; Technology White Papers nr. 3," *Cientifica Oct*, 2003.

[62] B. Clay, "Focus 2002: Consumer specialities: Technology Watch: Nanocrystalline materials for personal care," *Chem. Mar. Rep.*, **262** FR6 2002.

[63] W. G. Kreyling, M. Semmler-Behnke, W. Möller, "Health implications of nanoparticles," *J. Nano. Res.*, **8** 543 2006.

[64] P. Maestro, Y. Bomal, T. Chopin, "Nanoparticles in chemistry and their industrial applications," *Nanotech. 2006.*, **1** 332 2006.

[65] D. Tsoukalas, P. Dimitrakis, S. Kolliopoulou, P. Normand, "Recent advances in nanoparticle memories," *Mat. Sci. Eng. B*, **124-125** 93 2005.

[66] Q. Chen, M. Tanaka, K. Furuya, "Application of a UHV-MBE-TEM system on the deposition and HRTEM study of indium nanoparticles," *J. Surf. Anal.*, **5** 348 1999.

[67] K. Soulantica, L. Erades, M. Sauvan, F. Senocq, A. Maisonnat and B. Chaudret, "Synthesis of indium and indium oxide nanoparticles form indium cyclopentadienyl precursor and their applications for gas sensing," *Adv. Funct. Mater.*, **13** 553 2003.

[68] Y. Zhao, Z. Zhang, H. Dang, "A Novel Solution Route for Preparing Indium Nanoparticles," *J. Phys. Chem. B*, **107** 7574 2003.

[69] L. Zhang, H. Fu, C. Zhang, Y. Zhu, "Synthesis, Characterization, and Photocatalytic Properties of InVO4 Nanoparticles," *J. Solid State Chem.*, **179** 804 2006.

[70] J. Wang, G. Liu, Q. Zhu, "Indium microrod tags for electrochemical detection of DNA hybridization," *Anal. Chem.*, **75** 6218 2003.

[71] A. Cirpan and F. E. Karasz, "Indium Tin Oxide nanoparticles as anode for light-emitting diodes," *J. App. Poly Sc.*, **99** 3125 2006.

[72] P. K. Khannaa, K. W. Juna, K. B. Honga, J. O. Baega, R.C. Chikatea, B.K. Das, "Colloidal synthesis of indium nanoparticles by sodium reduction method," *Mat. Lett.*, **59** 1032 2005.

[73] Z. Li, X. Tao, Y. Chengb, Z. Wu, Z. Zhang, H. Danga, "A simple and rapid method for preparing indium nanoparticles from bulk indium via ultrasound irradiation," *Mat. Sc. Eng. A*, **407** 7 2005.

[74] R. A. Ganee, A. I. Ryasnyanskiy, U. Chakravarty, P. A. Naik, H. Srivastava, M. K. Tiwari, P. D. Gupta, "Structural, optical, and nonlinear optical properties of indium nanoparticles prepared by laser ablation," *Appl. Phys. B*, **86** 337 2007.

[75] K. Soulantica, A. Maisonnat, M. C. Fromen, M. J. Casanove and P. Lecante, "Synthesis and Self-Assembly of Monodisperse Indium Nanoparticles Prepared from the Organometallic Precursor [In(η^5-C5H5)]," *Angew. Chem. Int. Ed. Engl*, **40** 448 2001.

[76] D. Chen andY. Huang, "Spontaneous formation of Ag nanoparticles in dimethylacetamide solution of poly(ethylene glycol)," *J. Coll. Inter. Sc.*, **255** 299 2002.

[77]   B. C. Kim and D. W. Chae, "Effects of Zinc Oxide Nanoparticles on the Physical Properties of Polyacrylonitrile," *J. App. Poly. Sc.*, **99** 1854 2006.

[78]   H. Kleine, R. Wilke, C. Pelargus, K. Rott, A. Pühler, G. Reiss, R. Ros and D. Anselmetti, "Absence of intrinsic electric conductivity in single dsDNA molecules," *J. Biotech.*, **112** 91 2004.

[79]   A. Bensimon, A. Simon, A. Chiffaudel, V. Croquette, F. Heslot, D. Bensimon, "Alignment and sensitive detection of DNA by a moving interface," *Science*, **265** 2096 1994.

[80]   J. M. Schurr and S. B. Smith, "Theory for the extension of a linear polyelectrolyte attached at one end in an electric field," *Biopolymers*, **29** 1161 1990.

[81]   T. T. Perkins, S. R. Quake, D. E. Smith and S. Chu, "Relaxation of a single DNA molecule observed by optical microscopy," *Science*, **264** 822 1994.

[82]   A. Bezryadin, A. Bollinger, D. Hopkins, M. Murphey, M. Remeika, A. Rogachev, "Superconducting nanowires templated by single molecules," *Dekker Encyclopedia of Nanoscience and Nanotechnology*, . ed J. A. Schwarz, C. I. Contescu and K. Putyera (New York: Dekker), 3761 2004.

[83]   M. Mertig, L. C. Ciacchi, R. Seidel, W. Pompe, "DNA as selective metalization template," *Nano. Lett.*, **2** 841 2002.

[84]   O.   Harnack,   W.   E.   Ford,   A.   Yasuda,   J.   M.   Wessels, "Tris(hydroxymethyl)phosphine-capped gold particles templated by DNA as nanowire precursors," *Nano. Lett.*, **2** 91 2002.

[85]   C. F. Monson, A. T. Wooley, "DNA-templated construction of copper nanowires," *Nano. Lett.*, **3** 359 2003.

[86]   H. A. Becerril, R. M. Stoltenberg, C. F. Monson, A. T. Woolley, "Ionic surface masking for low background in single- and double-stranded DNA-templated silver and coppor nanorods," *J. Mater. Chem.*, **14** 611 2004.

[87]   Q. Gu, C. Cheng, D. T. Haynie, "Cobalt metallization of DNA: toward magnetic nanowires," *Nanotechnology*, **16** 1358 2005.

[88]   Q. Gu, C. Cheng, S. Suryanarayanan, K. Dai, D. T. Haynie, "DNA-templated fabrication of nickel nanocluster chains," *Physica E.*, **33** 92 2006.

[89]   P. Aich, S. L. Labiuk, L. W. Tari, L. J. T. Delbaere, W. J. Roesler, K. J. Falk, R. P. Steer and J. S. Lee, "A Complex Between Divalent Metal Ions and DNA which Behaves as a Molecular Wire," *J. Mol. Bio.*, **294** 477 1999.

[90]   J. S. Lee, L. J. P. Latimer, R. S. Reid, "A cooperative conformational change in duplex DNA induced by Zn^{2+} and other divalent metal ions," *Biochem. Cell. Biol.*, **71** 162 1993.

[91]   J. Wu, F. Du, P. Zhang, I. A. Khan, J. Chen, Y. Liang, "Thermodynamics of the interaction of aluminum ions with DNA: implications for the biological function of aluminum," *J. Inorg. Biochem.*, **99** 1145 2005.

[92]   G. Cervantes, V. Moreno, M. J. Prieto, "Study of DNA-interactions of new Pt(II) and Pd(II) complexes," *J. Inorg. Biochem.*, **59** 148 1995.

[93]   Y. Song, X. Lu, M. Yang, X. Zheng, "Study on the interaction of platinum(IV), gold(III) and silver(I) ions with DNA," *Trans. Metal Chem.*, **30** 499 2005.

[94]   J. Marmur, "A procedure for the isolation of deoxyribonucleic acid from microorganisms," *J. Mol. Bio.*, **3** 208 1961.

[95]   M. J. Waring, "Complex formation between ethidium bromide and nucleic acids," *J. Mol. Biol.*, **1** 269 1965.

[96]   J. Marmur and P. Doty, "Determination of the base composition of deoxyribonucleic acid from its thermal denaturation temperature," *J. Mol. Biol.*, **5** 109 1962.

[97]   J. Applequist, "Estimation of base pairing in nucleic acids from hypochromism," *J. Am. Chem. Soc.*, **83** 3158 1961.

[98]   G. Felsenfeld and S. Z. Hirschmann, "A neighbor-interaction analysis of the hypochromism and spectra of DNA," *J Mol Biol.*, **13** 407 1965.

[99]   M. N. Lipsett, "Aggregation of Guanine Oligoribonucleotides and the Effect of Mercuric Salts," *J. Bio. Chem.*, **239** 1250 1964.

[100]   S. A. Ross, M. Pitie, B. Meunier, "Synthesis of two acridine conjugates of the bis(phenanthroline) ligand clip-phen and evaluation of the nuclease activity of the corresponding copper complexes," *Euro. J. Inorg. Chem.*, **1999** 557 1999.

[101]   M. Tabata, A. K. Sarker, E. Nyarko, "Enhanced conformational changes in DNA in the presence of mercury(II), cadmium(II) and lead(II) porphyrins," *J. Inorg. Biochem.*, **94** 50 2003.

[102]   V. I. Ilvanov, L. E. Minchenkova, A. K. Schyolkina, A. I. Poletayev, "Different conformations of double-stranded nucleic acid in solution as revealed by circular dichroism," *Biopolymers.*, **12** 89 1973.

[103]   J. C. Sutherland, K. P. Griffin, P. C. Keck and P. Z Takacs, "Z-DNA: vacuum ultraviolet circular dichroism.," *Proc. Nat. Acad. Sci. USA*, **78** 4801 1981.

[104]   R. F. Pasternack and E. J. Gibbs, "Metal-DNA Chemistry," *ACS Symposium Series*, **402** 59 1989.

[105]   R. J. Fiel, "Porphyrin-nucleic acid interactions: a review," *J Biomol Struct Dyn.*, **6** 1259 1989.

[106]   C. V. Chrysikopoulos and P. Kruger, "Tech Report: Stanford Geothermal Program Interdisciplinary Research in Engineering and Earth Science," *SGP-TR-099* 38 1986.

[107]   R. Gonela, "Fabricating DNA-templated indium nanowires," M.S. Thesis, Louisiana Tech University, August, 2004.